Unclassified

SECURITY CLASSIFICATION OF THIS PAGE

REPORT DOCUMENTATION PAGE

1a. REPORT SECURITY CLASSIFICATION Unclassified	1b. RESTRICTIVE MARKINGS
2a. SECURITY CLASSIFICATION AUTHORITY	3. DISTRIBUTION/AVAILABILITY OF REPORT Approved for public release; distribution is unlimited.
2b. DECLASSIFICATION/DOWNGRADING SCHEDULE	
4. PERFORMING ORGANIZATION REPORT NUMBER(S)	5. MONITORING ORGANIZATION REPORT NUMBER(S)
6a. NAME OF PERFORMING ORGANIZATION Naval Postgraduate School 6b. OFFICE SYMBOL (*If applicable*) ME	7a. NAME OF MONITORING ORGANIZATION Naval Postgraduate School
6c. ADDRESS (*City, State, and ZIP Code*) Monterey, CA 93943-5000	7b. ADDRESS (*City, State, and ZIP Code*) Monterey, CA 93943-5000
8a. NAME OF FUNDING/SPONSORING ORGANIZATION 8b. OFFICE SYMBOL (*If applicable*)	9. PROCUREMENT INSTRUMENT IDENTIFICATION NUMBER
8c. ADDRESS (*City, State, and ZIP Code*)	10. SOURCE OF FUNDING NUMBERS Program Element No. / Project No. / Task No. / Work Unit Accession Number

11. TITLE (*Include Security Classification*)
NATURAL CONVECTION FROM A HORIZONTAL HEATER IN RESPONSE TO STEADY AND PULSATILE INPUT POWERS

12. PERSONAL AUTHOR(S) CHRISTOPHER N. HICKEY

13a. TYPE OF REPORT	13b. TIME COVERED	14. DATE OF REPORT (*year, month, day*)	15. PAGE COUNT
Master's Thesis	From To	JUNE 1992	84

16. SUPPLEMENTARY NOTATION
The views expressed in this thesis are those of the author and do not reflect the official policy or position of the Department of Defense or the U.S. Government.

17. COSATI CODES			18. SUBJECT TERMS (*continue on reverse if necessary and identify by block number*)
FIELD	GROUP	SUBGROUP	NATURAL CONVECTION HEAT TRANSFER, HORIZONTAL FLUSH HEATER STEADY AND PULSATILE INPUT POWERS

19. ABSTRACT (*continue on reverse if necessary and identify by block number*)

Natural convection heat transfer from a flush mounted heater on a larger horizontal substrate in water has been investigated for both steady state and periodic input powers. For steady power conditions, the heat flux was varied from 222 to 6880 W/m^2. Heater surface temperatures were measured at several locations in order to develop a non-dimensional heat transfer correlation. Three types of periodic input powers were tested: a triangular wave, an approximate square wave, and a sinusoidal wave. Mean, amplitude, and frequency were varied for each wave. Temperature measurements at selected heater locations were compared with steady state conditions to determine heat transfer enhancement.

20. DISTRIBUTION/AVAILABILITY OF ABSTRACT	21. ABSTRACT SECURITY CLASSIFICATION	
☒ UNCLASSIFIED/UNLIMITED ☐ SAME AS REPORT ☐ DTIC USERS	UNCLASSIFIED	
22a. NAME OF RESPONSIBLE INDIVIDUAL YOGENDRA JOSHI	22b TELEPHONE (*Include Area code*) (408) 646-3400	22c. OFFICE SYMBOL ME/Ji

DD FORM 1473, 84 MAR — 83 APR edition may be used until exhausted. All other editions are obsolete

SECURITY CLASSIFICATION OF THIS PAGE
Unclassified

Approved for public release; distribution is unlimited.

Natural Convection from a Horizontal Heater in Response
to Steady and Pulsatile Input Powers

by

Christopher N. Hickey
Lieutenant, United States Navy
B.S.O.E., United States Naval Academy, 1985

Submitted in partial fulfillment
of the requirements for the degree of

MASTER OF SCIENCE IN MECHANICAL ENGINEERING

from the

NAVAL POSTGRADUATE SCHOOL
June, 1992

ABSTRACT

Natural convection heat transfer from a flush mounted heater on a larger horizontal substrate in water has been investigated for both steady and periodic input powers. For steady power conditions, the heat flux was varied from 222 to 6880 W/m^2. Heater surface temperatures were measured at several locations in order to develop a non-dimensional heat transfer correlation. Three types of periodic input powers were tested: a triangular wave, an approximate square wave, and a sinusoidal wave. Mean, amplitude, and frequency were varied for each wave. Temperature measurements at selected heater locations were compared with steady state conditions to determine heat transfer enhancement.

TABLE OF CONTENTS

ACKNOWLEDGMENT

I would like to express my gratitude to Professor Joshi for his patience and guidance throughout this project. I would also like to thank Jim Scholfield and Tom Christian for their technical assistance.

I. INTRODUCTION

A. ELECTRONIC COOLING

With the continuing increase in the volumetric heat generation rates, heat removal from electronic components has become an important concern. For the first generation digital computers, forced air convection was employed to cool vacuum tubes used for basic logic elements. With the invention of the transistor in 1947, physical size of computers was reduced while reliability and performance were increased. In 1960, the monolithic circuit technology was introduced. With this technology, now fully integrated on a silicon chip, large scale integration has increased from 1000 gates per chip in the 1970s to upwards of 100,000 gates per chip in the 1980s. This trend towards higher packaging densities and the increase in power needed to accommodate the number of gates per chip has in turn increased the rate of heat generation.[Ref. 1] It is critical to maintain operating chip temperatures typically below 85°C since the average failure rates increase exponentially with junction temperatures.[Ref. 2]

As volumetric heat generation rates increase, forced air cooling is quickly reaching its full potential in many applications. Direct liquid cooling has emerged as one of the most promising heat removal techniques for future generation

electronic systems. Inert dielectric fluids such as the Fluorinert family are now commercially available for such applications.[Ref. 3]

Direct liquid cooling encompasses both single phase, natural, mixed and forced convection as well as phase change schemes. Both forced convection and phase change schemes are currently active areas of research. These methods can potentially increase heat removal by several orders of magnitude, over air cooling.[Ref. 1] While liquid immersion natural convection provides enhancements only moderate compared to boiling or forced convection, it has the advantages of simplicity of design, low maintenance, no noise and high reliability.[Ref. 4]

Recent studies on mixed and forced convective heat transfer for electronic cooling are discussed by Incropera [Ref. 5]. A number of studies on natural convection liquid immersion cooling have also been carried out. Joshi et. al. [Ref. 6] studied flow patterns and surface temperatures for liquid cooling of a 3 by 3 array of protruding heaters in an enclosure. Kelleher et. al. [Ref. 7] studied flows and heat transfer due to a long heated protrusion on a vertical insulated wall in a rectangular chamber filled with water. Lee et. al. [Ref. 8] using numerical computations supported Kelleher's findings for this case. Oosthuizen and Paul [Ref. 9] numerically examined the transport for a square protrusion mounted on the wall of an inclined square enclosure. Sathe and

Joshi [Ref. 4] computed the conjugate heat transfer from a protruding heat source on a vertical plate within an enclosure.

Joshi and Knight [Ref. 10] investigated a column of eight, flush mounted heat sources on a vertical wall in water. Gaiser [Ref. 11] investigated a three column array of 15 heaters per column, flush mounted on a vertical wall in water, while Haukenes [Ref. 12] numerically modeled a single substrate mounted flush heater. For flush heat sources on a vertical surface Akdeniz [Ref. 13] and Larsen [Ref. 14] investigated surface temperature responses for step and periodic input powers.

B. NATURAL CONVECTION ABOVE A HORIZONTAL HEATED FLAT PLATE

Goldstein et. al. [Ref. 15] used mass transfer experiments to correlate heat transfer from a heated isothermal upward-facing plate or a cooled downward-facing plate. These experiments were performed using a naphthalene sublimation technique. A comparison of the experimental results to a number of other studies was presented. The deviations were attributed to differences in experimental procedures and geometric configurations.

Lloyd and Moran [Ref. 16] also studied natural convection mass transfer from a horizontal flat plate. An electrochemical technique was used to measure mass transfer. Their correlation for laminar mass transfer agreed with the measurements of

Goldstein et. al. [Ref. 15]. A correlation for turbulent mass transfer was also developed.

Husar and Sparrow [Ref. 17] preformed flow visualizations for the above configurations. Their results showed that a boundary layer develops normal to each edge of the plate. As these boundary layers grow over the plate, the adjacent boundary layers eventually collide. The line of collision bisects the angle between the connecting edges. Ackroyd [Ref. 18] performed an analytical study using the boundary region flow described by Husar and Sparrow. These results were compared with available experimental data and reasonable agreement was found.

C. OBJECTIVES

The present study consisted of two parts. The first was to evaluate the thermal characteristics of buoyancy induced flow resulting from a discrete flush mounted heat source on a larger horizontal substrate. While the transport characteristics for a fully heated horizontal surface have been investigated, very little information is available for a heated surface surrounded by an un-heated area. The second objective was to investigate the effects of a pulsatile input power on the heat transfer characteristics.

Specific goals of this study were:

- To design and build the test surface consisting of a horizontal substrate and heater assembly.

- Experimentally determine surface temperature distributions at various steady power settings and develop a corresponding heat transfer correlation.
- To determine the effects of pulsating input power on the heat transfer characteristics.

II. EXPERIMENTAL APPARATUS AND PROCEDURES

A. EXPERIMENTAL APPARATUS

The experimental apparatus is sub-divided into four separate assemblies; the test surface assembly, the power supply assembly, the data acquisition/reduction unit, and the deaeration/filtration assemblies, as seen in Figure 1. The first three assemblies are interrelated through distinct variables; the input power to the heater, the temperature measurements on the test surface, and the ambient temperature of the bath. The fourth system deals with the purification of the water and the removal of entrained air.

The data acquisition system, water tank, and water filtration system are described in detail by Gaiser [Ref. 11]. Additions and modifications to the apparatus were discussed by Haukenes [Ref. 12], Akdeniz [Ref. 13], and Larsen [Ref. 14]. The following is a summary of the above with particular emphasis on the modifications which reflect the current status of the apparatus.

1. Test Surface Assembly

The test surface assembly consisted of a horizontal test surface with a flush mounted heater centrally imbedded within a larger substrate. The substrate was constructed using a 30.48 cm x 30.48 x 0.64 cm plexiglass board with an 11.0 cm

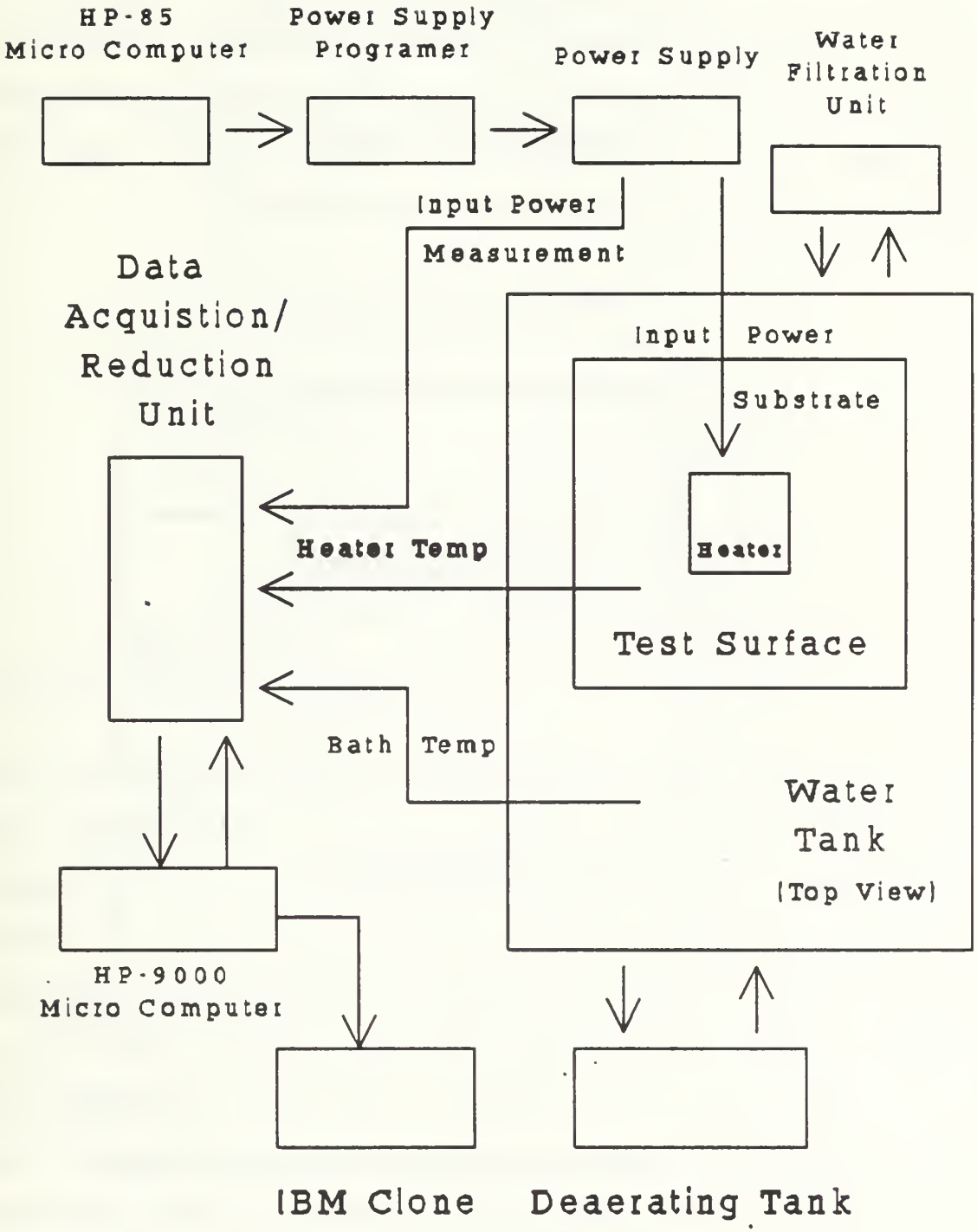

Figure 1. Experimental Apparatus

square milled out to a depth of 0.178 mm where the heater is mounted. A top view of the surface showing the location of the heater is shown in Figure 2. Within the square, a number of holes were drilled and channels were milled out to accommodate the power leads and thermocouple wires, Figure 3 shows the size and locations of the holes and channels.

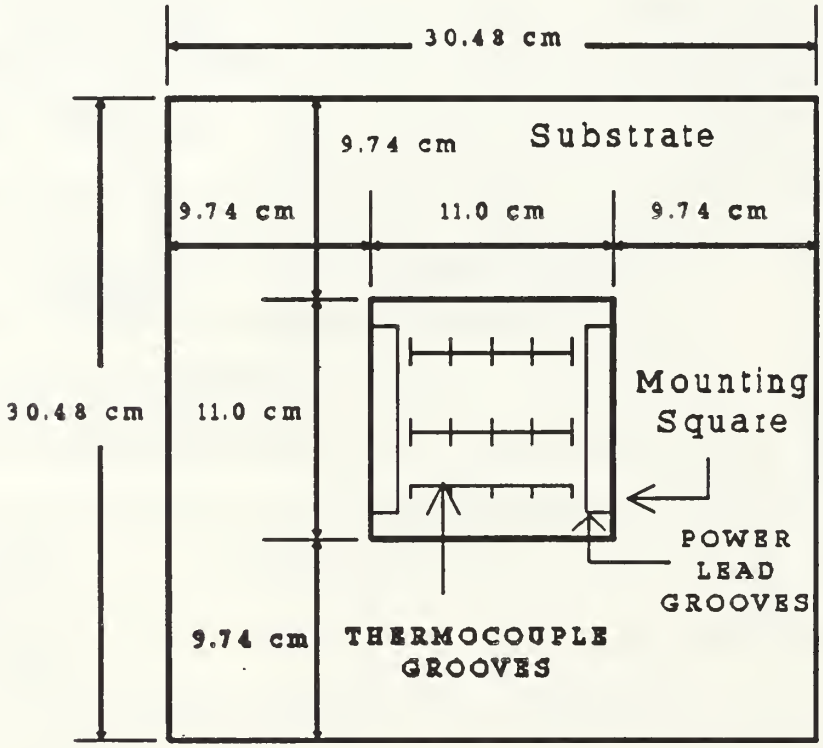

Figure 2. Top View of the Substrate and Mounting Square

The heater is a gold/tin oxide film sputtered on a nylon substrate manufactured by Courtaulds Performance Films (Courtaulds' FM-1). The net thickness of the film and substrate was 0.165 mm. It had a surface resistance of 2.6 ohms/square. The film was etched so that only a 10.0 cm x 9.0

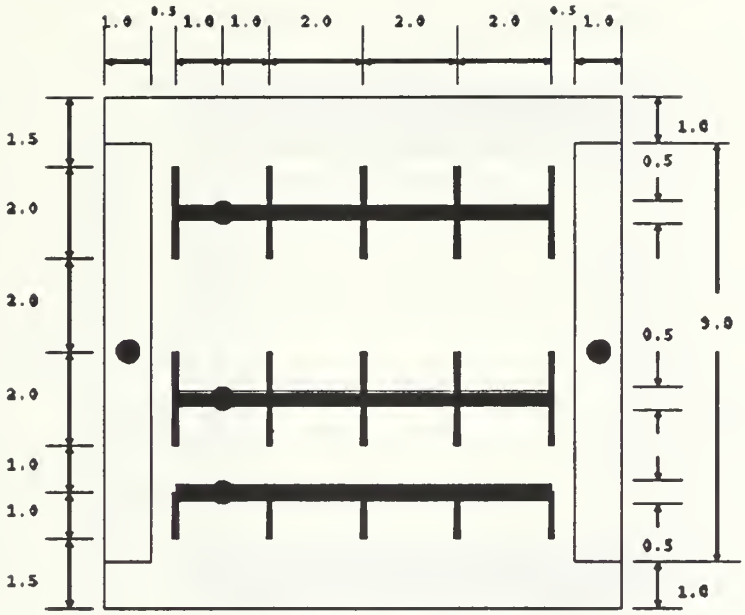

Figure 3. Mounting Square

cm portion remained coated with the gold/tin oxide. The film was then cut to an 11 cm square. The power leads were connected to the film with the use of a silver loaded "ink" which has a low electrical resistance, approximately 0.2 ohms/square. The "ink" overlapped the gold/tin oxide by 0.5 cm on each side, making the heated area a 9.0 cm square as seen in Figure 4.

Before mounting the heater plate to the board, twenty five 0.013 cm copper-constantan thermocouples were attached to the substrate plate at precise locations. Figure 5 identifies each thermocouple and its location on the plate. The

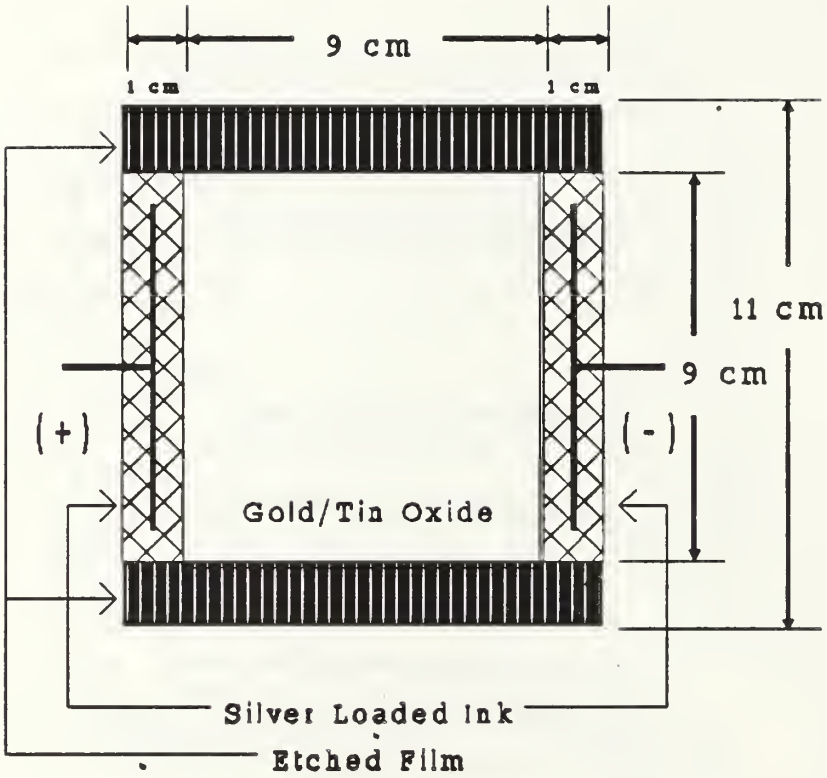

Figure 4. Bottom View of Test Heater

thermocouples were placed through the drilled holes, set in the channels, and attached to the plate with Omega Bond 101, a high thermal conductivity adhesive. Attaching the thermocouples in this manner electrically isolates them from the heater while still allowing for accurate temperature measurements.

In order to construct a flush test surface, great care had to be used in mounting the test heater. A thin film of Omega Bond 101 was spread over the milled square on the substrate plate. The power leads were then placed through the drilled holes and the test heater was lowered into the

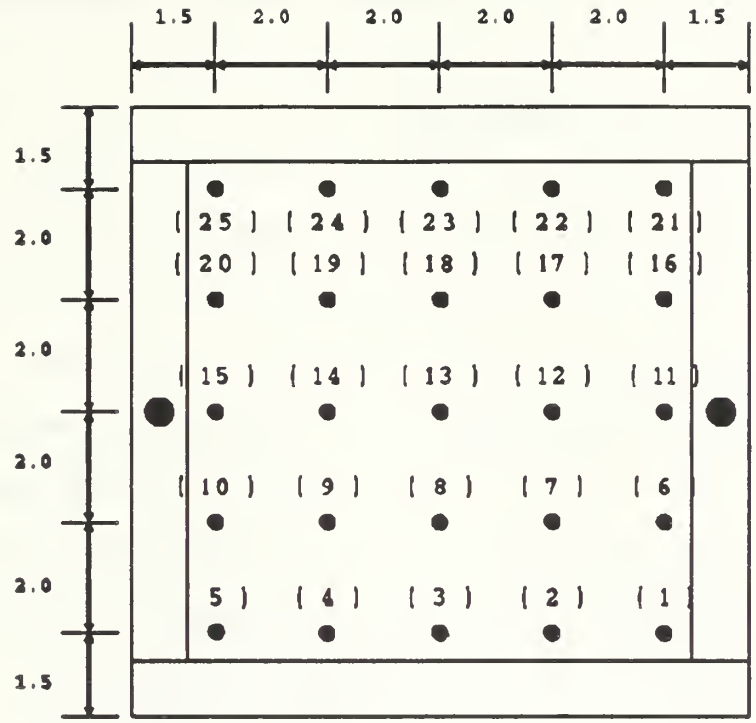

Figure 5. Location of the Thermocouples on the Test Heater

substrate. A roller was used to smooth out the surface and displace any air bubbles which might have been trapped between the heater and the substrate. This was allowed to cure for 12 hours with a flat weight holding it in place. A 0.013 cm sheet of thermochromic liquid crystal (TLC) was attached over the entire test surface for the visualization of the temperature patterns. The crystals in this sheet displayed shades of yellow, green, and blue in reaction to temperature changes in the approximate range of 28° to 34° C. The crystals were calibrated in place against the 25 thermocouples in air. Calibration data were taken at the color start temperatures.

Based on these, yellow appears at approximately 28°C, green at 30°C, blue-green at 32°C, and dark blue at temperatures above 34°C.

2. Power Supply Assembly

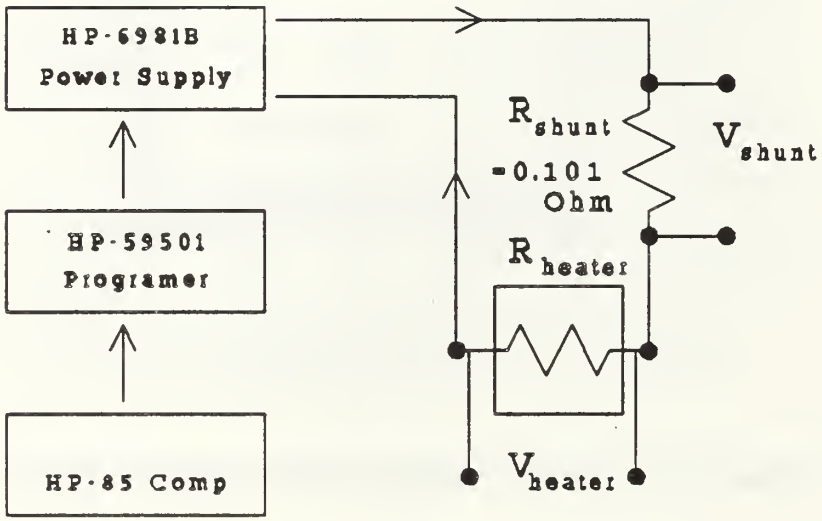

Figure 6. Power Supply Assembly

This was the portion of the experimental apparatus which provided power to the heater. The power supply assembly consisted of a Hewlett Packard(HP)-85 computer used in conjunction with an HP-59501 power supply programmer and a 0-20 Volt, 0-10 Amp HP-6286A D.C. power supply to control the input power to the heater. The power assembly was connected in

series with a 0.101 Ohm precision shunt, and the heater as shown in Figure 6.

3. Data Acquisition/Reduction Assembly

The data acquisition/reduction assembly was fully explained in Larsen [Ref. 14], the following is a brief summary of his description. The assembly consisted of a HP 3852A Data Acquisition unit, a HP 9153 Computer system, and an IBM clone personal computer. The computer controlled the data acquisition system, instructing it to monitor desired thermocouples and measure the voltage drops across the heater. With the voltage reading across the precision shunt (V_{shunt}) and the heater (V_{heater}) known, along with the resistance of the shunt (R_{shunt}), the input power to the heater was easily computed by the following equation:

$$Power = \left(\frac{V_{shunt}}{R_{shunt}}\right) V_{heater}$$

After processing the data, it was transferred to the IBM clone where it was imported into a spread sheet program for graphics.

4. Deaerating/Filtration Assembly

The deaerating unit consisted of a vacuum pump, a discharge pump, a heating element, and the deaerating tank. While in operation, a pressure of between 68 and 85 KPa was maintained inside the tank creating a vacuum. The heating element raised the water temperature 10 - 15 K above the bulk

temperature in the tank. Water is pulled into the deaerating tank by vacuum drag and discharged through the discharge pump. [Ref. 14]

The filtration system consisted of four cartridge filters used to maintain the resistivity of the tank water above 0.7 megaohm-cm. Figure 7 shows the combination of both

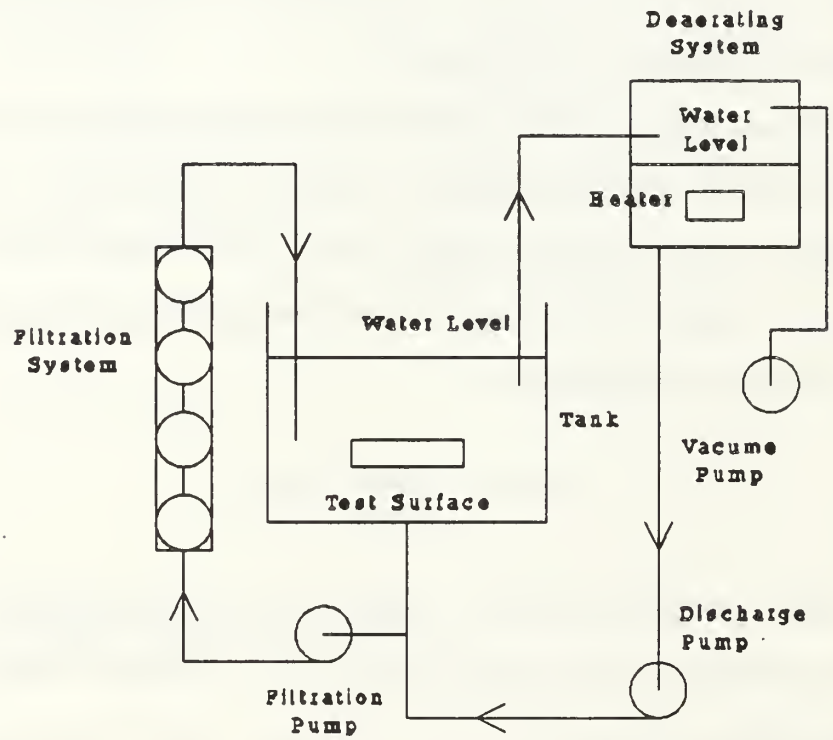

Figure 7. Deaerating/Filtration Assembly

the deaerating and filtration systems.

B. EXPERIMENTAL PROCEDURE

The experimental program consisted of two parts, the first involving steady input powers and the second pulsatile input powers. For both parts, the bath was prepared in the same manner. A mechanical stirrer was run for five to ten minutes to dissipate temperature stratification within the test tank. The tank was then allowed to reach quiescence, which took approximately 30 minutes. The computers and data acquisition system were then turned on and allowed to warm up.

To initiate a typical run, a program used to generate a steady heater power input was loaded and run. For the first part, the heater was allowed to reach steady state, which took approximately 15 minutes. The data acquisition program was then run and temperatures at the 25 locations were measured over a nine minute period. This was done for eleven different power levels. Runs at four different power levels were performed twice, in order to confirm repeatability of data. The resulting temperatures were within 1.3%.

For the second part of the study, the steady power program was again run for about ten minutes to warm up the heater. Following this, a program used to generate the appropriate periodic power input pattern was loaded and run. The heater was then allowed to reach a periodic steady state. The data acquisition program was then run and periodic temperature measurements were taken over a six minute period.

Three different types of periodic input power patterns were examined: a triangular wave, an approximate square wave, and a sinusoidal wave. For each run measurements at five different thermocouple locations, #13, #14, #15, #19, and #25 in Figure 5, were obtained. The locations were selected as representative ones for the entire test surface. These measurements were obtained for three mean input power levels, each with three frequencies. Two mean input powers had four amplitude variations and one had two amplitude variations.

During both parts of the investigation, temperature patterns were visualized at the 19.8 watt power level using the thermochromic liquid crystal (TLC) sheet.

III STEADY STATE RESULTS AND DISCUSSION

A. DATA ANALYSIS

A simple energy balance around the heater neglecting conduction losses, yields the convective rate of heat loss:

$$Q_{conv}=Q_{heat}$$

Where Q_{heat} is the power supplied to the heater in watts.

With Q_{conv} defined, the non-dimensional heat transfer coefficient based on the heat flux, Nusselt number (Nu) and the Rayleigh number (Ra), can be calculated. The Nusselt number was defined as:

$$Nu=\frac{Q_{conv}L_c}{kA(T_{plate}-T_{amb})}$$

T_{plate} is the average of all twenty five thermocouples over the nine minute scan period. L_c is the characteristic length equal to the ratio of the surface area to the perimeter of the heater. The Rayleigh number is given by:

$$Ra=\frac{g\beta Q L_c^4}{kA\nu^2}Pr$$

All fluid properties used in the data reduction were determined at a film temperature assumed as the average of the plate temperature (T_{plate}) and the ambient fluid temperature (T_{amb}).

The Nusselt number results from the present investigation are plotted in Fig. 8 as a function of the Rayleigh number.

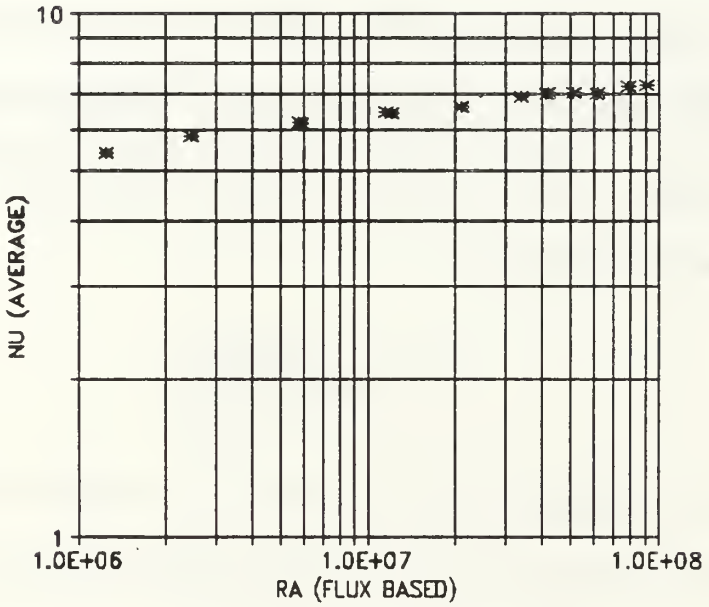

Figure 8. Average Nusselt Number Versus The Heat Flux Based Rayleigh Number

The resultant correlation of the data is assumed to follow the general relation:

$$Nu = a(Ra)^{n}$$

The values of a and n are determined from a linear best fit for the data plotted in Fig. 8. The resulting correlation is:

$$Nu = 2.22(Ra)^{.065}$$

This equation is valid for $1.2x10^{6} < Ra < 9.1x10^{7}$.

In an attempt to correlate the present results with previously developed correlations found by Lloyd and Moran [Ref. 16] a temperature based Rayleigh number was defined. Assuming T_{plate} to be the constant plate temperature, the Rayleigh number was calculated using:

$$Ra_{T_{plate}} = \frac{g\beta L_c^3 (T_{plate} - T_{amb})}{\nu^2} Pr$$

The results found in Lloyd and Moran differed from those found in this investigation. Figure 9 shows a graphical comparison of the two results. Variations in the geometry of the test surfaces could account for the large differences in the results. Lloyd and Moran tested a fully heated surface, while the surface used in the present investigation had an unheated area surrounding it.

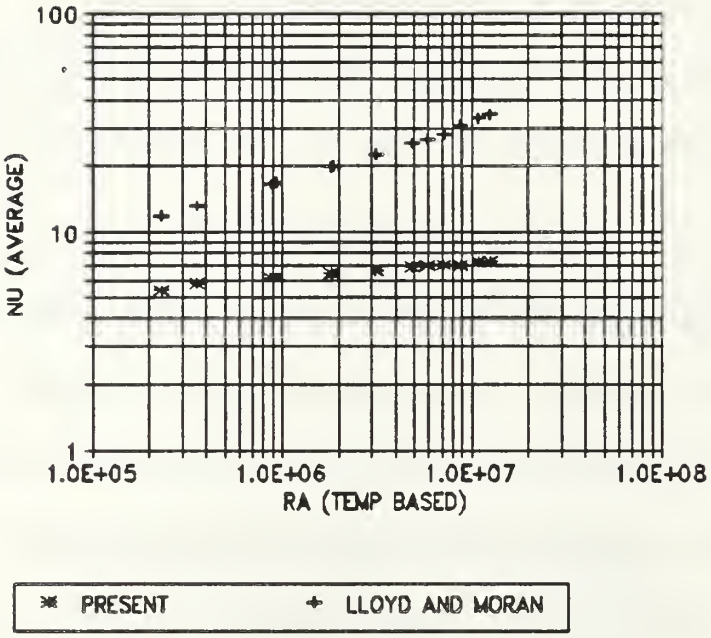

Figure 9. Comparison of Steady Data With Constant Temperatures

B. SURFACE TEMPERATURE PATTERNS AND THERMOCOUPLE MEASUREMENTS

Before the discussion of the present results, the flow patterns found by Husar and Sparrow [Ref. 17] must be mentioned. The basic characteristic found was the partitioning of the natural convection flow field for surfaces with corners. Boundary layers were initiated perpendicular to the edges of the plate. The adjoining boundary layers intersect forming a partition. For a square, the partitioned areas are shaped as isosceles right triangles. The partition nearly coincides with the bisectors of the angles of the plate. No

flow crosses a partition line, but rather each partition line is a central element of a vertical ascending buoyant plume. These lines are not fixed, but show some waviness as a result of the meandering nature of the rising plume.

Surface temperature patterns in the present study were visualized using a liquid crystal sheet. Shades of yellow, green, and blue were observed over approximately a 6°C

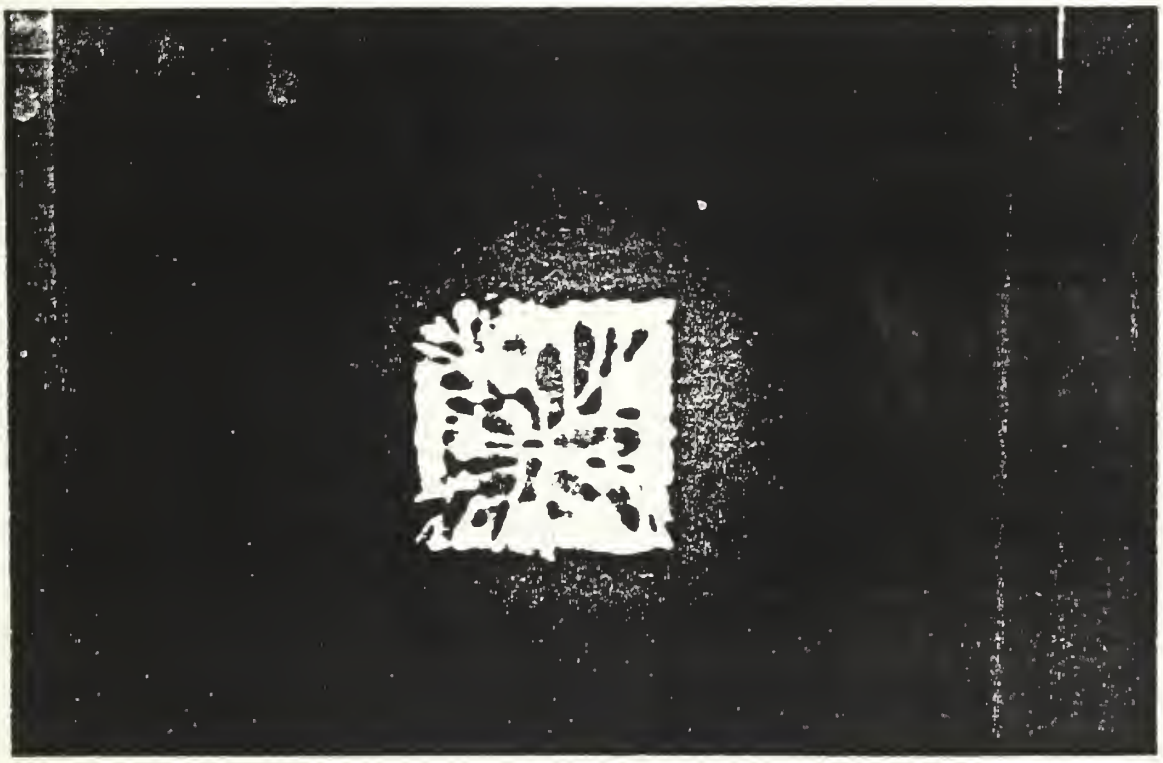

Figure 10. Heated Portion of the Plate

bandwidth above 28°C. Figure 10 shows a picture of the liquid crystal display at a heat flux of 2440 W/m² and a flux based

Rayleigh number of 2.1×10^7 . The crystals displayed a dark blue area, about 1 cm in width, just inside the edge of the heated portion of the plate. This area remained rather constant showing no changes in color during the testing. Partitioning was also observed by blue lines nearly coinciding with the bisectors of the corners. Blue lines were also seen at discrete locations within the partitioned areas. These lines are also part of the ascending buoyant plume, appearing to entrain the heated surrounding fluid up into the plume. This leaves a cooler area adjacent to the lines thus accounting for the green, yellow and black colors seen in the center of the plate. Both the partition lines and the lines within the partitioned area meandered around slightly but still maintained the general form of the isosceles right triangle. The visual results of Husar and Sparrow [Ref. 17] at the same Rayleigh number were very similar.

Temperature measurements over the plate support the visual results. The temperatures obtained around the edge of the plate were on an average higher and more steady than that at the center. The temperature within the center showed fluctuations over time. This is due to the partition lines and

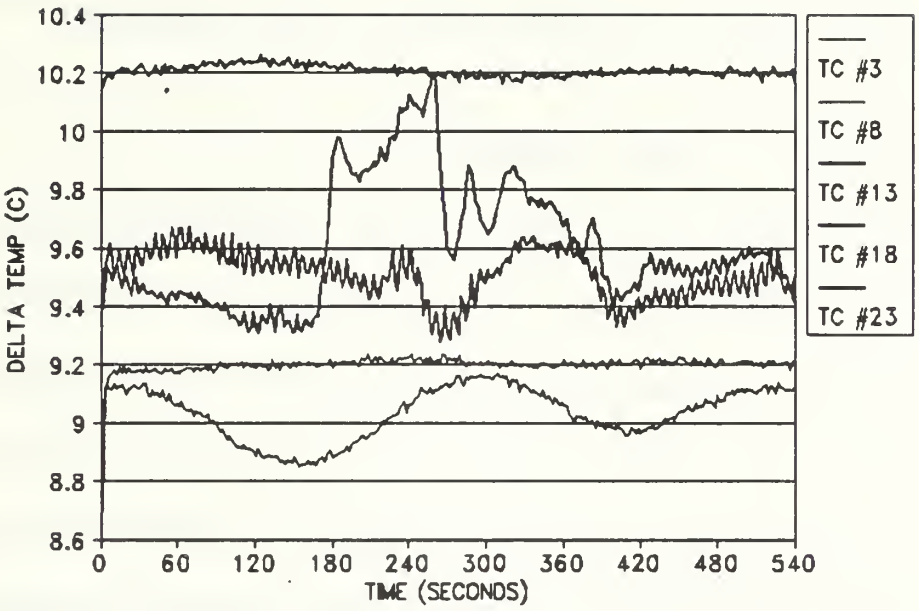

Figure 11. Temperatures of a Cross Section of the Plate

the lines within the partitioned areas meandering over the temperature sensor. Figure 11 shows a plot of the temperatures at an input power of 19.8 W for a cross section of the plate. The thermocouple locations are #3, #8, #13, #18, and #23.

IV PULSATILE POWER RESULTS AND DISCUSSION

A. DESCRIPTION OF DATA PRESENTATION

This portion of the investigation studied the effects of different pulsatile input powers on heat transfer. Three power patterns in the forms of a triangular wave, a sinusoidal wave, and a square wave were examined. Two amplitudes for the mean power level of 3.2 W and four amplitude variations for the mean levels of 19.8 W and 59.6 W were studied. Within this

Table I. Combinations of mean input power and amplitude to mean power ratios.

MEAN (Watts)	AMPLITUDE TO MEAN (R)		RATIO	
3.20	1.25	2.00		
19.80	0.202	0.404	0.707	1.010
59.6	0.081	0.161	0.282	0.402

chapter a combination of the mean power and the amplitude to mean power ratio will be used for identification of each run. Table I lists these combinations. For each of the ten combinations three different frequencies were used, 0.025 Hz, 0.050 Hz, and 0.10 Hz.

Temperature measurements were taken at five discrete locations over the plate. Due to the partitioning of the plate discussed previously, the locations chosen were #13, #14, #15, #19, and #25 in Figure 5. Thermocouples #19 and #25 are on the bisecting angle of the corner, while #14 and #15 are within the partitioned area. Thermocouple #13 is at the center of the test heater. These locations will be subsequently referred to by their numbers.

Heat transfer enhancement will be referred to by an enhancement parameter (E). This is defined as the ratio of the mean temperature level at a location due to steady power input to the mean temperature level at the same location due to pulsatile power input. Values of $E>1$ indicate beneficial effects of pulsation while $E\leq1$ implies no benefit due to the pulsation. Appendix A contains a complete listing of all runs performed and resulting values of E. Appendix B is an example of the graphical data that were obtained. The combination presented is for a mean power of 19.8 W and a mean to amplitude ratio of 0.707.

B. RESULTS FOR A MEAN POWER OF 3.2 WATTS

Two amplitudes were used for this mean power level, 4.0 W amplitude, corresponding to R=1.25, and a 6.2 W amplitude or R=2.0.

For both amplitudes with the triangular wave pattern, the greatest enhancement was for 0.10 Hz, while the 0.050 Hz had the least. The smaller amplitude also had a larger effect on the enhancement. The sinusoidal wave showed similar enhancement characteristics but not to the same degree. The enhancement for both the 0.10 Hz and the 0.025 Hz patterns was the same. The 0.050 Hz pattern still had the least enhancement but it was better than for the corresponding triangular wave. An example of this is shown in Figures 12 and 13. The amplitude change had little effect on the sine wave. The square wave did not follow this trend. Rather, little to no enhancement was seen in the smaller amplitude, while enhancement in the range of E= 1.069 to 1.231 was noticed in the larger amplitude. The 0.10 Hz again had the greatest enhancement and the 0.025 Hz had the least.

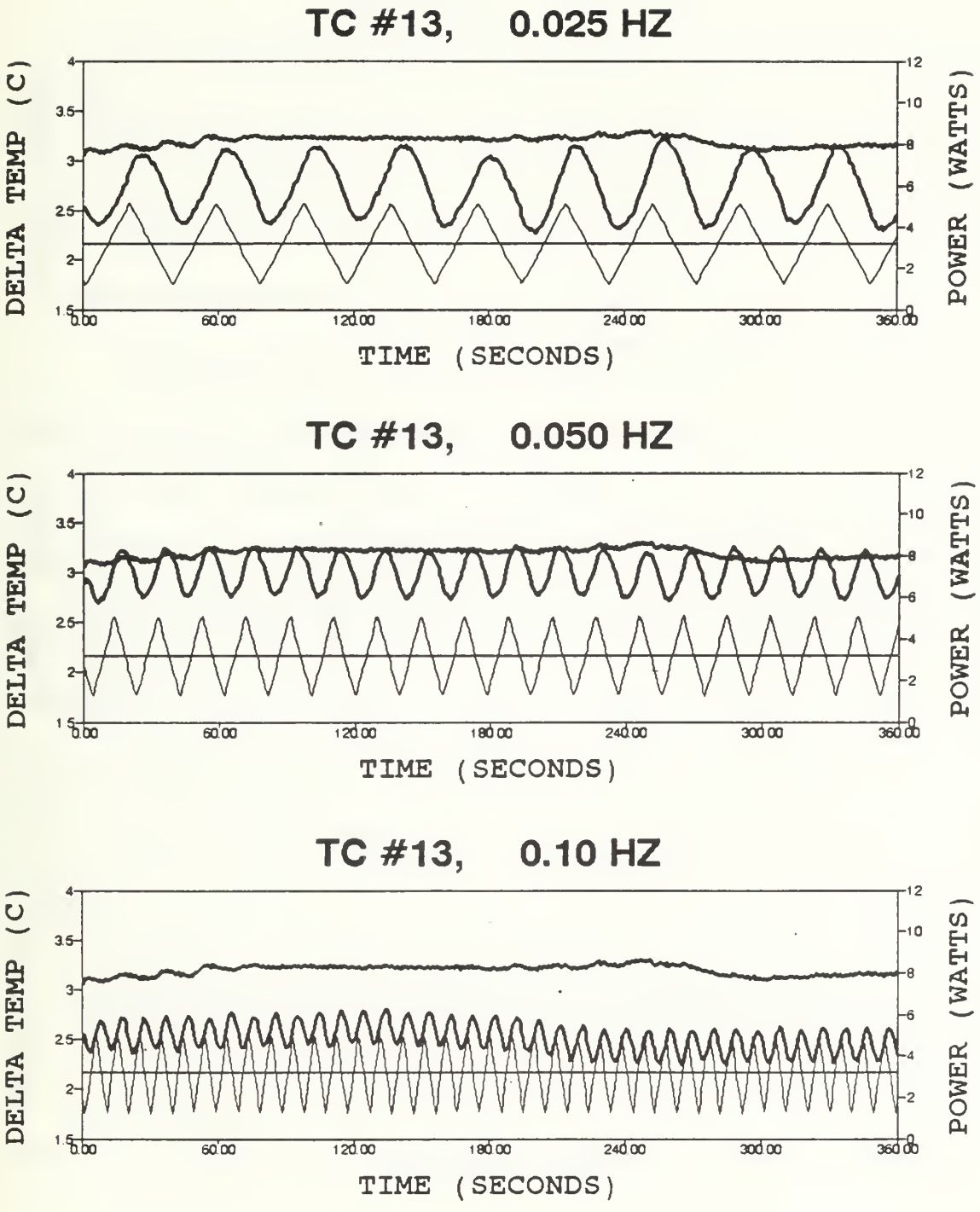

Figure 12. Delta temperature response for steady and cyclic input with triangular wave pattern at #13 for 3.2 W and R=1.25. Bold=Delta temp response, Fine=Power input.

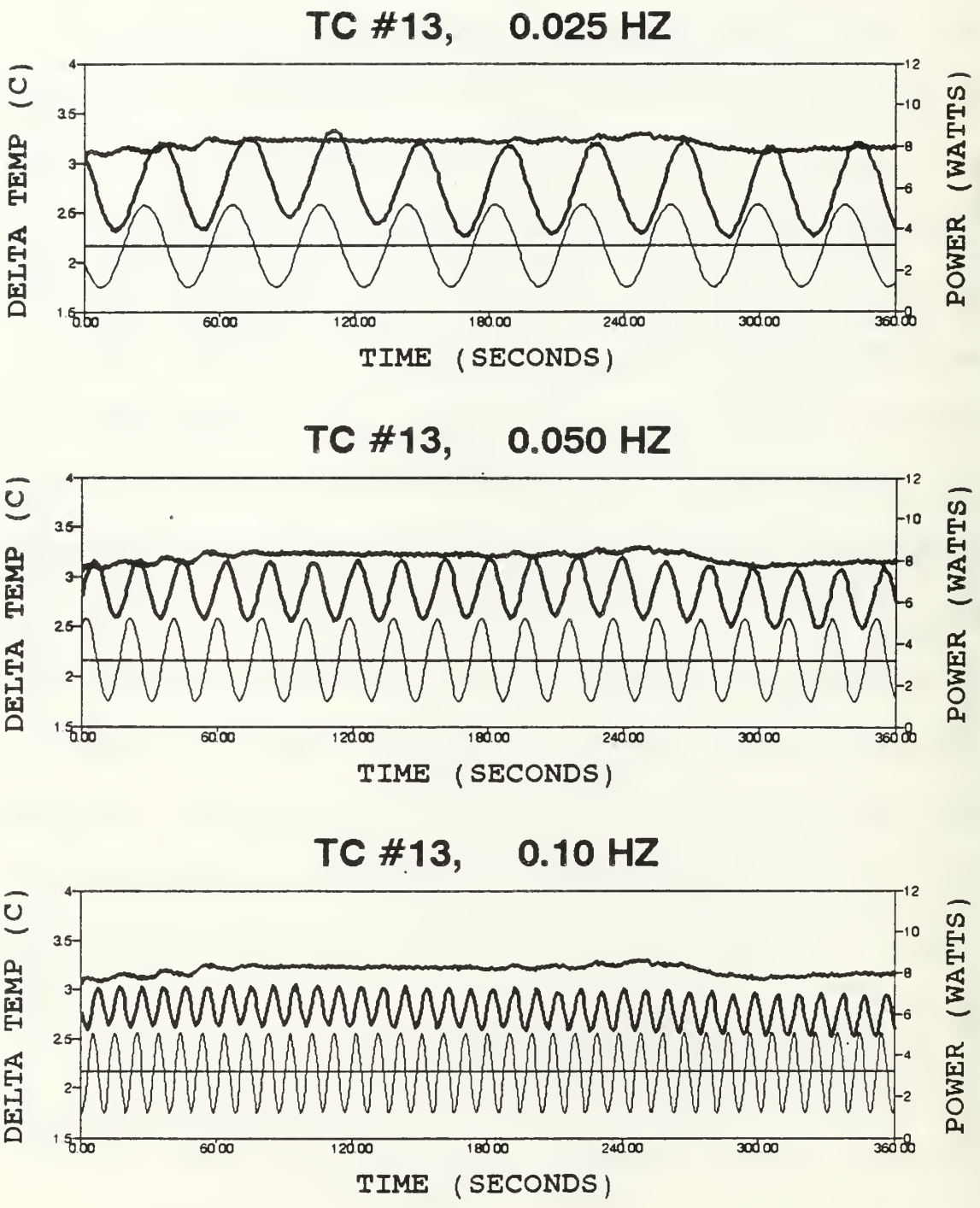

Figure 13. Delta temperature response for steady and cyclic input with sinusoidal wave pattern at #13 for 3.2 W and R=1.25. Bold=Delta temp response, Fine=Power input.

1. Amplitude to Mean Power Ratio of 1.25

For the triangular wave, the heat transfer enhancement characteristics at all five locations followed the trend just discussed. All three frequencies had enhancement. The values of E ranged from 1.291 at thermocouple #19 for 0.10 Hz to 1.036 at thermocouple #14 for 0.050 Hz.

With some minor variations, the sinusoidal wave showed similar characteristics. Enhancement was found at location #s 13, 15, 19, and 25 for all frequencies. The enhancement parameters for these four locations were the same for both 0.10 Hz and 0.025 Hz. The 0.050 Hz again showed the least enhancement. Location #14 only had enhancement for 0.025 Hz. $E \leq 1$ was seen at the other two frequencies. The range of E was from 1.148 at #19 for 0.025 Hz and 0.10 Hz to 0.967 at #14 for 0.10 Hz.

Location #s 14 and 19 , with the square wave, had $E<1$ for all three frequencies. Locations showing enhancement were #s 13, 15, and 25 at 0.025 Hz and at #13 for 0.10 Hz. E ranged from 1.067 at #13 for 0.10 Hz to 0.912 at #19 for 0.10 Hz.

2. Amplitude to Mean Power Ratio of 2.0

For the triangular wave all five locations, again, had enhancement for all three frequencies except for location #s 13, 14, and 25 at 0.050 Hz. There was no enhancement (E=1) at location #s 13 and 25, while #14 had E<1. The values of E ranged from 1.142 at #13 for 0.10 Hz to 0.967 at #14 for 0.050 Hz.

The sinusoidal wave, had E>1 at all five locations for all frequencies. At location #s 13, 15, 19, and 25 the enhancement parameters were independent of the frequencies. The enhancement parameter at #14 was the same for 0.050 Hz and 0.025 Hz, while for 0.10 Hz it increased slightly. The parameter E ranged from 1.148 at #19 to 1.036 at #14.

The square wave data showed enhancement at all five locations for 0.050 Hz and 0.10 Hz. For the 0.025 Hz frequency, enhancement was seen at #s 13 and 15, while E<1 was seen at #s 14 and 19. E ranged from 1.231 at #13 for 0.10 Hz to 0.935 at #14 for 0.025 Hz.

C. MEAN POWER OF 19.8 WATTS

Four amplitudes were used for this mean power level. These included 4.0 W (R=0.202), 8.0 W (R=0.404), 14.0 W (R=0.707), and 20.0 W (R=1.01).

Enhancement for this mean input appeared to be dependent on a combination of both amplitude and frequency for the triangular and sinusoidal waves. As the amplitude increased, enhancement was noticed as the frequencies increased. The upper end of this trend seemed to be near the 14.0 W amplitude, because the 20.0 W amplitude response was similar to that at the lowest amplitude. These conditions are seen in the sine wave's graphical data for location #13, Figures 14-17. The square wave response was again quite different. Certain conditions exhibited enhancement, but no particular pattern was noticed.

1. Amplitude to Mean Power Ratio of 0.202

For the triangular wave, only location #s 15 and 25 for 0.025 Hz had enhancement. Location #s 13 and 19 had no enhancement (E=1) for the same frequency. All other locations and frequencies resulted in E<1. The enhancement parameter E ranged from 1.007 at location #s 15 and 25 to 0.958 at #s 14

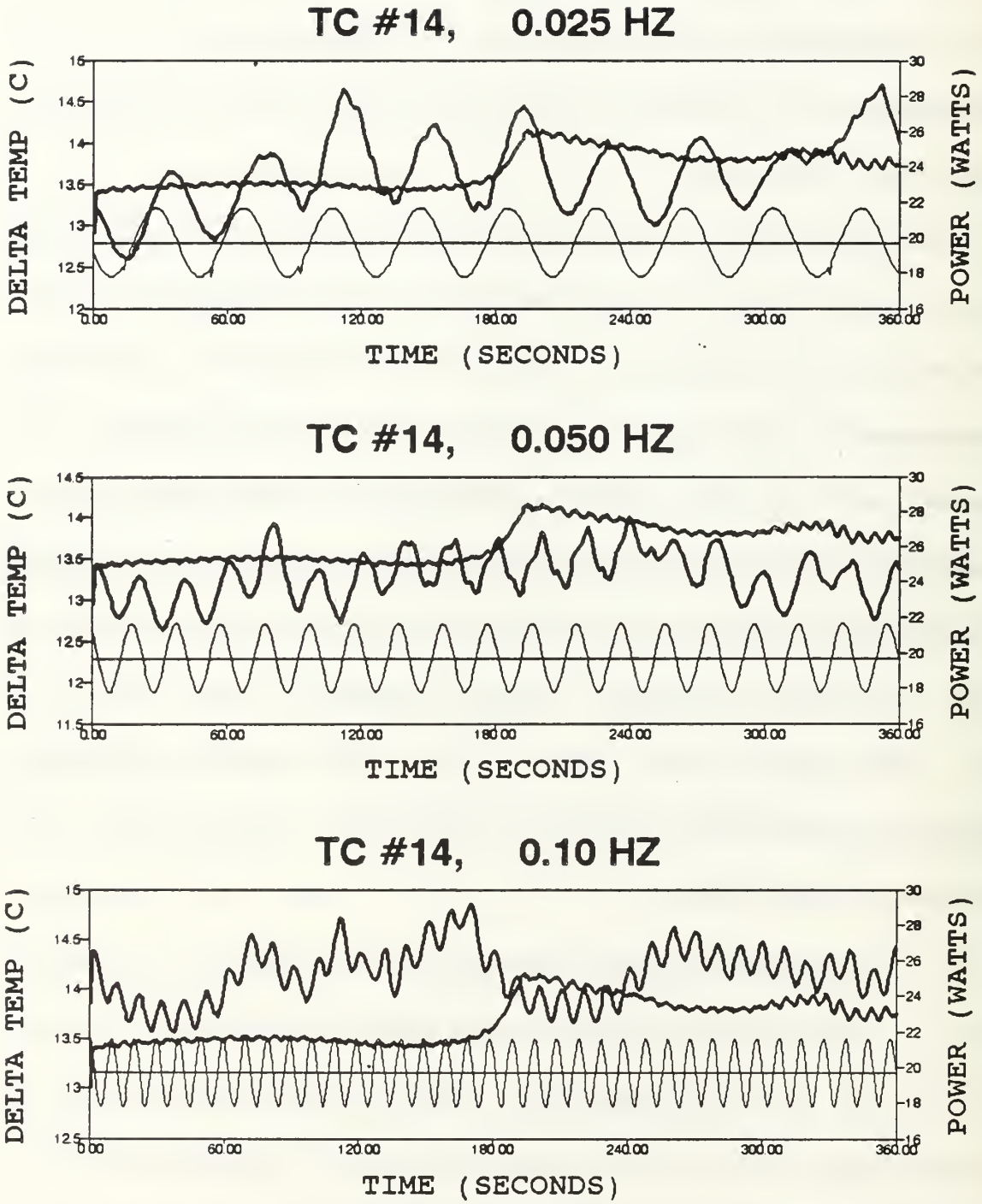

Figure 14. Delta temperature response for steady and cyclic input with sinusoidal wave pattern at #14 for 19.8 W and R=0.202. Bold=Delta temp response, Fine=Power input.

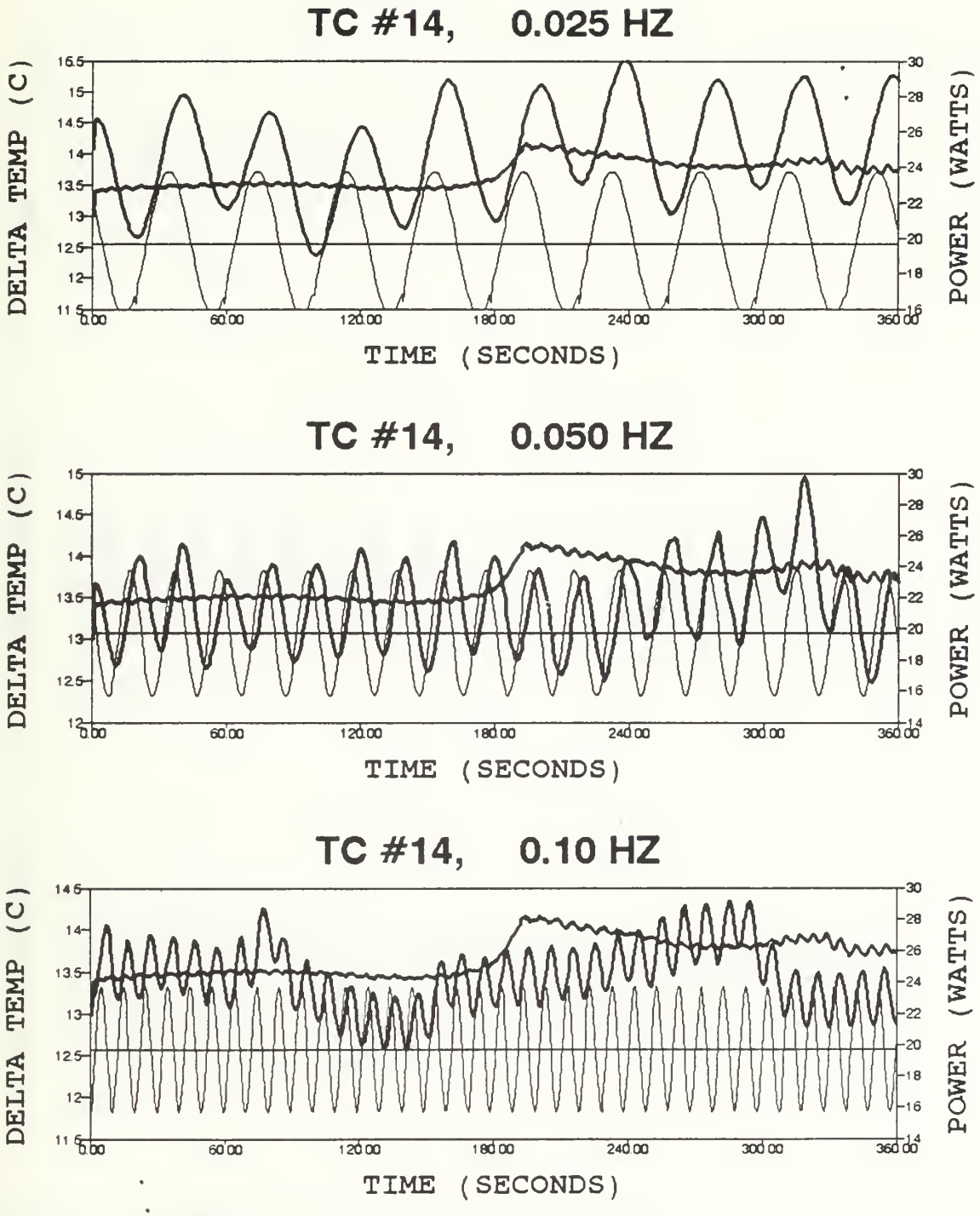

Figure 15. Delta temperature response for steady and cyclic input with sinusoidal wave pattern at #14 for 19.8 W and R=0.404. Bold=Delta temp response, Fine=Power input

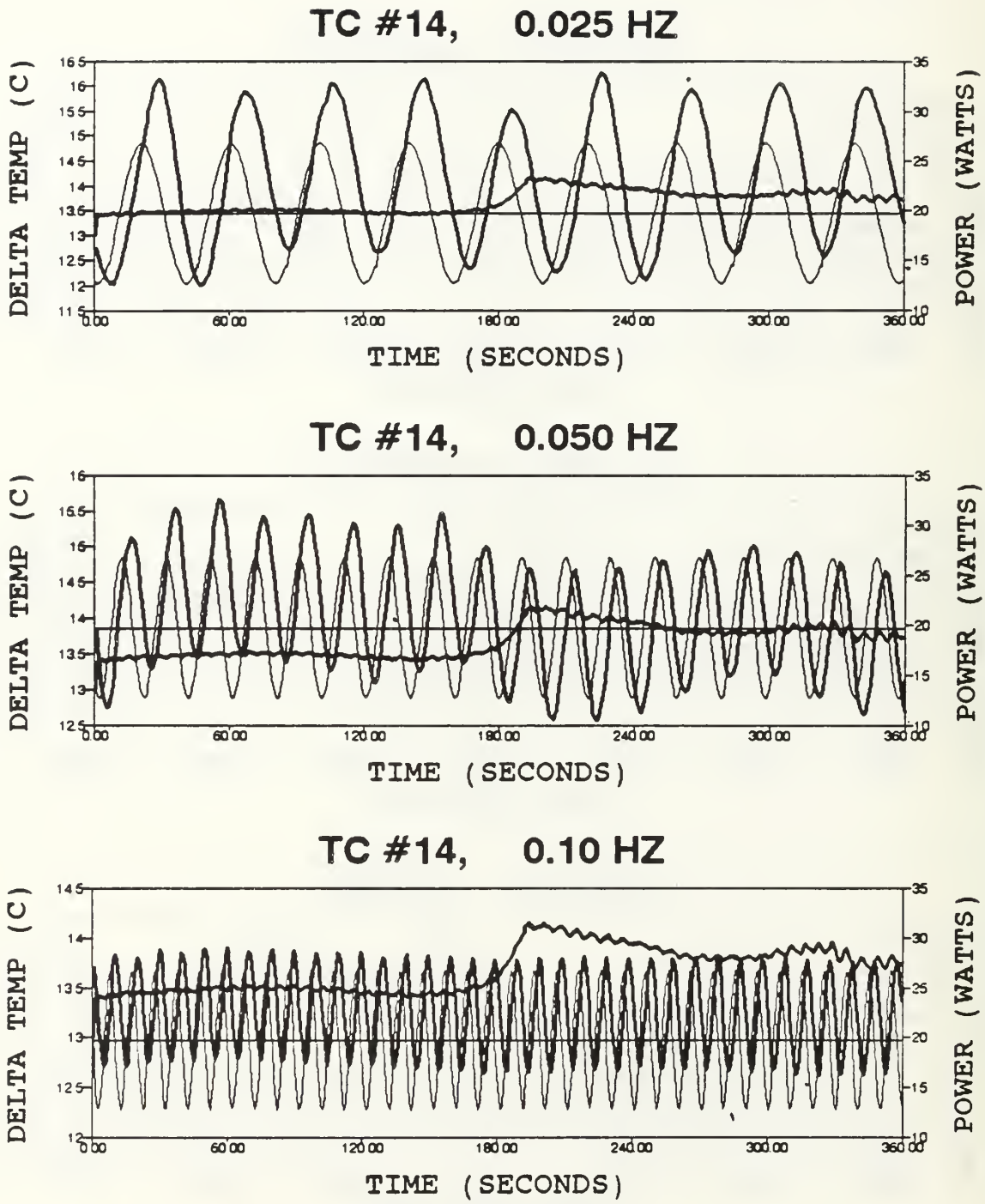

Figure 16. Delta temperature response for steady and cyclic input with sinusoidal wave pattern at #14 for 19.8 W and R=0.707. Bold=Delta temp response, Fine=Power input

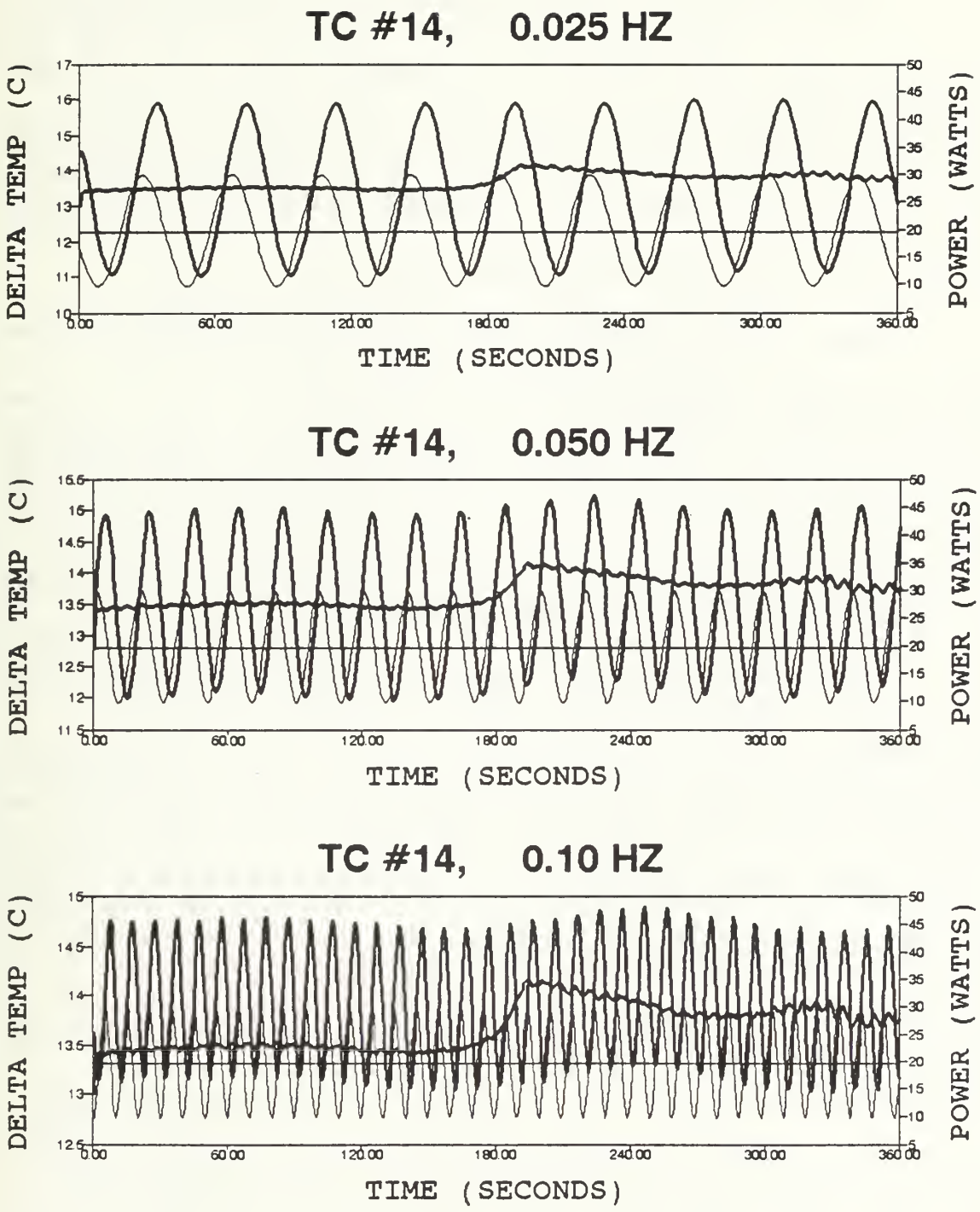

Figure 17. Delta temperature response for steady and cyclic input with sinusoidal wave pattern at #14 for 19.8 W and R=1.010. Bold=Delta temp response, Fine=Power input

and 19 for 0.050 Hz.

The sinusoidal wave resulted in a slightly higher E value at some locations. At all locations for 0.025 Hz and 0.050 Hz E ranged from 1.0 at #19 for 0.025 Hz to 1.038 at #19 for 0.050 Hz. For the 0.10 Hz frequency all five locations had an E<1 with the lowest parameter being 0.965 at #14.

With the square wave, all five locations had E<1 for the two lowest frequencies. Only location #s 13, 14, 15, and 25 had E>1 for 0.10 Hz. The largest value of E was 1.022 at #14.

2. Amplitude to Mean Ratio of 0.404

With the triangular wave, all five locations showed enhancement for the frequencies of 0.050 Hz and 0.10 Hz. Location #25 also showed an enhancement for 0.025 Hz. No enhancement (E=1) was seen at #s 13 and 15, while #s 14 and 19 had E<1 for a 0.025 Hz frequency. This is a higher value of E compared to the response for R=0.202. E ranged from 1.022 at location #14 for 0.10 Hz to 0.986 at #14 for 0.025 Hz.

The sinusoidal wave, like the triangular wave, had E>1 at all five locations for the 0.050 Hz and 0.10 Hz frequencies. For 0.025 Hz E=1 at #s 15 and 25, while E<1 was

found for location #s 13, 14, and 19. E ranged from 1.043 at #25 for 0.10 Hz to 0.967 at #13 for 0.025 Hz.

The square wave had E<1 for all locations and all frequencies except at #25 for 0.025 Hz. E at this point was 1.007.

3. Amplitude to Mean Power Ratio of 0.707

The triangular wave had enhancement at all five locations for 0.10 Hz and at #15 for 0.050 Hz. For 0.025 Hz and at all other locations at 0.050 Hz, E was below 1. E ranged from 1.036 at #13 for 0.10 Hz to 0.965 at #14 for both 0.025 Hz and 0.050 Hz.

The sine wave, like the triangular wave, had enhancement at all locations for 0.10 Hz and at location #25 for 0.050 Hz. All other locations had E≤1. The E values ranged from 1.036 at #13 for 0.10 Hz to 0.965 at #14 for 0.025 Hz.

The frequencies of 0.025 Hz and 0.10 Hz with the square wave had enhancement at all locations. The 0.10 Hz frequency showed the greatest degree of enhancement, similar to the results found for the triangular and sinusoidal waves with a mean input of 3.2 W. Figure 18 is an example of this result at location #15. The 0.050 Hz had the smallest E

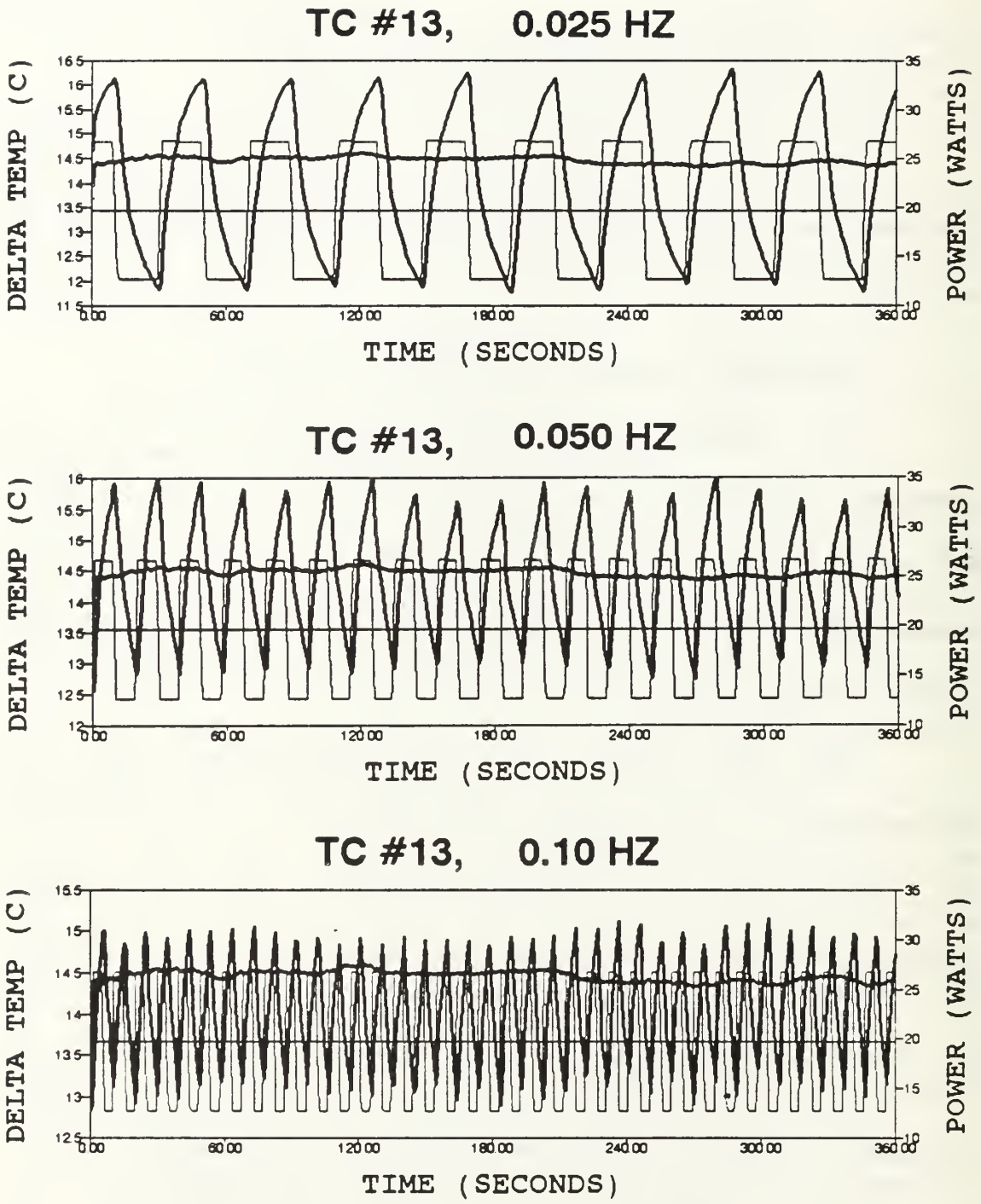

Figure 18. Delta temperature response for steady and cyclic input with square wave pattern at #13 for 19.8 W and R=0.707. Bold=Delta temp response, Fine=Power input

values, with E=1 at #25 and E<1 at #s 15 and 19. The parameter E ranged from 1.036 at #13 for 0.10 Hz to 0.986 at #15 for 0.025 Hz.

4. Amplitude to Mean Power Ratio of 1.01

The triangular wave showed enhancement at all locations for 0.025 Hz. The only other locations resulting in E>1 were location #s 13 and 25 for 0.050 Hz. No enhancement was seen at location #s 15 and 19 for 0.050 Hz. All other locations and frequencies had E<1. The range of E was from 1.036 at #13 for 0.050 Hz to 0.966 at #15 for 0.10 Hz.

For 0.025 Hz and 0.050 Hz, the sinusoidal wave resulted in enhancement at all locations except at #15. The frequency of 0.10 Hz had E≤1 for the five locations. The largest value of E was 1.015 at #14 for 0.025 Hz and 0.050 Hz.

The square wave showed enhancement at all locations for 0.025 Hz as well as at #13 for 0.050 Hz and at #s 13 and 14 for 0.10 Hz. E≤1 was seen at all other locations and frequencies. E ranged from 1.039 at #14 for 0.025 Hz to 0.979 at #15 for 0.050 Hz.

D. MEAN POWER OF 59.6 WATTS

Four amplitudes were used for this mean power level. These included 4.0 W (R=0.081), 8.0 W (R=0.161), 14.0 W (R=0.282), and 20.0 W (R=0.402).

Temperature response at this mean power level was more dependent on R rather than on the wave form or frequency of power pulsation. For this section comments on the results will be on responses at the spatial locations rather than on the wave forms. At location #s 13 and 25 for all four amplitude variations nearly all waves and frequencies resulted in $E<1$. Location #14, for the two smaller amplitudes, had $E<1$ for nearly all waves and frequencies. The two larger amplitudes, at this location, resulted in $E>1$ for nearly all waves and frequencies. Location #15 showed enhancement at the smaller amplitudes and degradation in heat transfer for the larger ones. Location #19 was the only location to display enhancement over the entire range of amplitudes. The only variation to the location dependency was the sinusoidal wave for the two smaller amplitudes. This resulted in $E\leq 1$ at most locations for all frequencies. The enhancement data in Appendix A presents these results best.

1. Amplitude to Mean Power Ratio of 0.081

At location #s 13 and 14, the wave and frequency combinations resulted in E<1, except for the 0.025 Hz triangular wave at #13. Location #15 showed enhancement except for the sinusoidal wave at all three frequencies. Location #19, like #15, had enhancement with the exception of the 0.025 Hz and 0.050 Hz sine patterns. At location #25, for triangular wave E increased from below 1 for 0.025 Hz to above 1 for 0.10 Hz. The sine wave again showed no enhancement for the three frequencies. The square wave only showed noticeable enhancement at 0.10 Hz.

2. Amplitude to Mean Power Ratio of 0.161

With the exception of the 0.10 Hz triangular wave, all wave form and frequency combinations resulted in E<1 for location #s 13 and 14. For location #15, except for the 0.025 Hz and 0.050 Hz sine wave, all the combinations had enhancement. At #19 the square wave resulted in enhancement with increase in frequency. The sinusoidal and triangular waves produced mostly deterioration in heat transfer. Except for the 0.025 Hz square wave pattern, E was below 1 at location #25.

3. Amplitude to Mean Power Ratios of 0.282 and 0.402

Heat transfer deterioration was seen at location #s 13, 15, and 25 for most wave and frequency combinations. The only exceptions were the 0.025 Hz square wave patterns of both amplitudes at #15 and the 0.10 Hz sine wave of R=0.402 at #13. Location #s 14 and 19 showed enhancement for most wave and frequency combinations, except the 0.025 Hz square wave with R=0.282.

V. CONCLUSIONS

Several important conclusions were drawn about the transfer of heat from a flush horizontal heat source. The addition of an unheated area surrounding a heater reduced the heat transfer coefficient compared to a fully heated surface with a steady input power. This was expected due to the development of the momentum boundary layer prior to the thermal layer development. Visualization of the surface temperature pattern indicate a similar partitioning effect within the fluid flow adjacent to the heated area as seen for a fully heated plate.

Introducing a pulsatile input power provided several interesting findings. The lowest mean power level produced the greatest enhancement parameters for all waves. The range of enhancement parameters for the medium and high mean inputs were similar to each other and noticeably lower than for the low mean input. Of the three wave forms, the triangular wave pattern displayed the largest degree of enhancement with a low mean input, low amplitude, and high frequency. For a vertical flush heater Larsen [Ref. 14] found the greatest enhancement

for the same pattern, frequency, and ratio, but for a higher mean input.

The triangular and sinusoidal wave inputs had similar enhancement patterns for the medium mean power input. At the intermediate R (0.404 and 0.707) enhancement was at the higher frequencies. At the highest R (1.010) enhancement was for the lower frequency. The square wave exhibited enhancement for certain conditions, but no predominant trend was noticed for either the low or medium mean power levels.

The enhancement at the high power level was dependent on location and amplitude ratio vice wave form. At low R (0.081 and 0.161), the center edge and regions along the partition line had enhancement. At the higher R (0.282 and 0.402) enhancement was around the center but some distance apart. With the ultimate objective of providing heat transfer enhancement characteristics for electronic components, the lower mean power level with a triangular wave pattern and a higher pulsation frequency holds the most promise.

VI. RECOMMENDATIONS

In continuation of this study it is recommended that the following aspects be further studied:

- Investigate the fluid flow adjacent to the surface and within the buoyant plume for steady and cyclic power inputs.
- The effects due to possible turbulent effects caused by increased amplitudes and mean power inputs.
- Numerically study the heat transfer characteristics corresponding to both steady and pulsatile inputs.
- Investigate the heat transfer adjacent to an inclined flush plate at various angles.
- The buoyant plume appears to initiate its ascent at the partition lines and the lines within the partitioned area. The meandering of these lines adjacent to the plate could possibly be controlled. The ascent may by mechanically initiated with raised lines along the bisectors and at discrete locations within the partitioned area. If the meandering is controllable, hot spots on the surface could be controlled. An investigation of this type should be done to determine the controllability of these lines.

APPENDIX A

LIST OF DATA RUNS AND ENHANCEMENT PARAMETERS

MEAN (W)	RATIO	WAVE	FREQUENCY (Hz)	VALUES OF E				
				#13	#14	#15	#19	#25
3.2	1.25	TRI	0.025	1.185	1.208	1.200	1.240	1.200
3.2	1.25	TRI	0.050	1.067	1.036	1.111	1.148	1.111
3.2	1.25	TRI	0.10	1.280	1.208	1.250	1.292	1.250
3.2	1.25	SIN	0.025	1.143	1.074	1.111	1.148	1.111
3.2	1.25	SIN	0.050	1.103	1.000	1.111	1.107	1.111
3.2	1.25	SIN	0.10	1.143	0.967	1.111	1.148	1.111
3.2	1.25	SQR	0.025	1.032	0.967	1.034	0.969	1.034
3.2	1.25	SQR	0.050	1.185	1.074	1.200	1.148	1.154
3.2	1.25	SQR	0.10	1.067	0.967	1.000	0.912	1.000
3.2	2.00	TRI	0.025	1.067	1.036	1.071	1.069	1.034
3.2	2.00	TRI	0.050	1.000	0.967	1.034	1.033	1.000
3.2	2.00	TRI	0.10	1.143	1.074	1.111	1.107	1.111
3.2	2.00	SIN	0.025	1.143	1.036	1.111	1.148	1.111
3.2	2.00	SIN	0.050	1.143	1.036	1.111	1.148	1.111
3.2	2.00	SIN	0.10	1.143	1.074	1.111	1.148	1.111
3.2	2.00	SQR	0.025	1.032	0.935	1.034	0.969	1.000
3.2	2.00	SQR	0.050	1.185	1.074	1.200	1.148	1.154
3.2	2.00	SQR	0.10	1.231	1.160	1.200	1.069	1.154

MEAN (W)	RATIO	WAVE	FREQUENCY (Hz)	VALUES OF E				
				#13	#14	#15	#19	#25
19.8	0.202	TRI	0.025	1.000	0.986	1.007	1.000	1.007
19.8	0.202	TRI	0.050	0.973	0.958	0.986	0.958	0.979
19.8	0.202	TRI	0.10	0.986	0.972	0.986	0.979	0.986
19.8	0.202	SIN	0.025	1.007	1.007	1.022	1.000	1.021
19.8	0.202	SIN	0.050	1.036	1.030	1.022	1.038	1.036
19.8	0.202	SIN	0.10	0.967	0.965	0.979	0.986	0.986
19.8	0.202	SQR	0.025	0.980	0.972	0.966	0.979	0.979
19.8	0.202	SQR	0.050	0.973	0.958	0.972	0.958	0.979
19.8	0.202	SQR	0.10	1.007	1.022	1.022	0.993	1.021
19.8	0.404	TRI	0.025	1.000	0.986	1.000	0.993	1.007
19.8	0.404	TRI	0.050	1.021	1.007	1.014	1.007	1.021
19.8	0.404	TRI	0.10	1.021	1.022	1.007	1.007	1.007
19.8	0.404	SIN	0.025	0.967	0.979	1.000	0.993	1.000
19.8	0.404	SIN	0.050	1.028	1.022	1.022	1.030	1.029
19.8	0.404	SIN	0.10	1.036	1.022	1.029	1.030	1.044
19.8	0.404	SQR	0.025	0.993	0.993	1.000	0.979	1.007
19.8	0.404	SQR	0.050	0.980	0.958	0.979	0.972	0.986
19.8	0.404	SQR	0.10	0.954	0.958	0.952	0.951	0.966

MEAN (W)	RATIO	WAVE	FREQUENCY (Hz)	VALUES OF E				
				#13	#14	#15	#19	#25
19.8	0.707	TRI	0.025	0.980	0.965	0.979	0.979	0.979
19.8	0.707	TRI	0.050	0.986	0.965	1.014	0.979	0.986
19.8	0.707	TRI	0.10	1.036	1.015	1.014	1.007	1.029
19.8	0.707	SIN	0.025	0.986	0.965	0.979	0.972	1.000
19.8	0.707	SIN	0.050	1.000	0.979	0.979	0.986	1.007
19.8	0.707	SIN	0.10	1.036	1.030	1.014	1.030	1.029
19.8	0.707	SQR	0.025	1.028	1.030	1.014	1.015	1.021
19.8	0.707	SQR	0.050	1.007	1.007	0.986	0.993	1.000
19.8	0.707	SQR	0.10	1.036	1.022	1.007	1.015	1.014
19.8	1.010	TRI	0.025	1.028	1.007	1.014	1.007	1.014
19.8	1.010	TRI	0.050	1.036	0.986	1.000	1.000	1.021
19.8	1.010	TRI	0.10	0.986	0.979	0.966	0.972	0.973
19.8	1.010	SIN	0.025	1.007	1.015	0.993	1.007	1.007
19.8	1.010	SIN	0.050	1.014	1.015	0.993	1.007	1.007
19.8	1.010	SIN	0.10	1.000	0.986	0.966	0.979	0.979
19.8	1.010	SQR	0.025	1.036	1.038	1.014	1.022	1.021
19.8	1.010	SQR	0.050	1.014	1.000	0.979	0.986	0.993
19.8	1.010	SQR	0.10	1.028	1.015	0.993	1.000	1.000

MEAN (W)	RATIO	WAVE	FREQUENCY (Hz)	VALUES OF E				
				#13	#14	#15	#19	#25
59.6	0.081	TRI	0.025	1.010	0.987	1.026	1.006	0.997
59.6	0.081	TRI	0.050	0.978	0.997	1.000	1.013	1.003
59.6	0.081	TRI	0.10	0.991	0.997	1.016	1.033	1.012
59.6	0.081	SIN	0.025	0.978	0.981	1.000	0.994	0.997
59.6	0.081	SIN	0.050	0.958	0.975	0.994	0.984	1.000
59.6	0.081	SIN	0.10	0.972	0.987	0.997	1.006	0.982
59.6	0.081	SQR	0.025	0.991	0.987	1.016	1.016	1.003
59.6	0.081	SQR	0.050	0.984	0.981	1.032	1.013	1.000
59.6	0.081	SQR	0.10	0.972	0.978	1.016	1.019	1.022
59.6	0.161	TRI	0.025	0.984	0.981	1.013	1.016	0.991
59.6	0.161	TRI	0.050	0.988	0.987	1.029	0.997	0.982
59.6	0.161	TRI	0.10	1.006	1.000	1.016	1.000	0.979
59.6	0.161	SIN	0.025	0.975	0.991	0.985	0.994	0.997
59.6	0.161	SIN	0.050	0.969	0.987	1.000	0.981	0.979
59.6	0.161	SIN	0.10	0.969	0.955	1.022	0.981	0.988
59.6	0.161	SQR	0.025	0.969	0.981	1.006	1.013	1.003
59.6	0.161	SQR	0.050	0.984	0.981	1.026	1.029	0.985
59.6	0.161	SQR	0.10	0.972	0.981	1.026	1.036	0.976

MEAN (W)	RATIO	WAVE	FREQUENCY (Hz)	VALUES OF E				
				#13	#14	#15	#19	#25
59.6	0.282	TRI	0.025	0.966	1.003	0.988	1.010	0.982
59.6	0.282	TRI	0.050	0.984	1.016	0.988	1.006	0.982
59.6	0.282	TRI	0.10	0.991	1.013	0.988	1.010	0.982
59.6	0.282	SIN	0.025	0.943	1.006	0.988	1.023	0.976
59.6	0.282	SIN	0.050	0.960	1.006	0.985	1.013	0.979
59.6	0.282	SIN	0.10	0.981	1.010	0.988	1.003	0.979
59.6	0.282	SQR	0.025	0.969	0.997	1.003	0.991	0.985
59.6	0.282	SQR	0.050	0.981	1.010	0.991	1.010	0.982
59.6	0.282	SQR	0.10	0.988	1.006	0.994	1.016	0.985
59.6	0.402	TRI	0.025	0.988	1.013	0.994	1.010	0.988
59.6	0.402	TRI	0.050	0.988	1.010	0.988	1.003	0.985
59.6	0.402	TRI	0.10	0.984	1.006	0.991	1.000	0.985
59.6	0.402	SIN	0.025	0.994	1.013	0.991	1.006	0.985
59.6	0.402	SIN	0.050	0.991	1.013	0.991	1.006	0.988
59.6	0.402	SIN	0.10	1.003	1.010	0.991	1.010	0.985
59.6	0.402	SQR	0.025	0.994	1.013	1.000	1.019	0.991
59.6	0.402	SQR	0.050	0.988	1.010	0.997	1.019	0.991
59.6	0.402	SQR	0.10	0.988	1.006	0.997	1.019	0.991

APPENDIX B

SAMPLE OF RESULTS IN GRAPHICAL FORM

Graphical data presented here is a sample of a complete set of runs for a mean power and R combination. A combination like this consists of data at all five locations for each wave pattern with each frequency. The combination here is a mean power of 19.8 W and a R of 0.707. The bold lines are the tempeature rise over ambiant levels for the power inputs indicated by the fine lines.

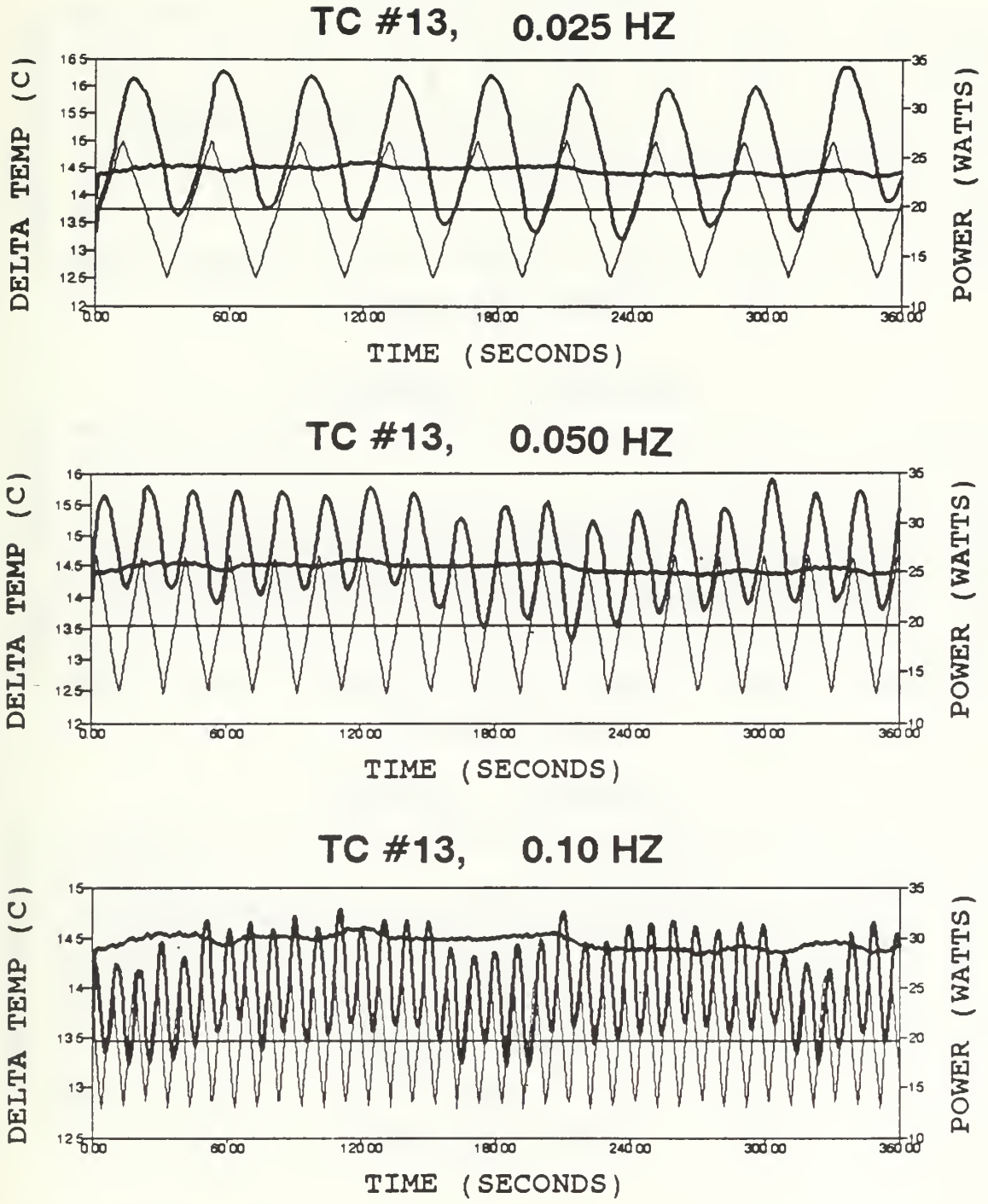

Figure 19. Delta temperature response for steady and cyclic input power with a triangular wave pattern at #13.

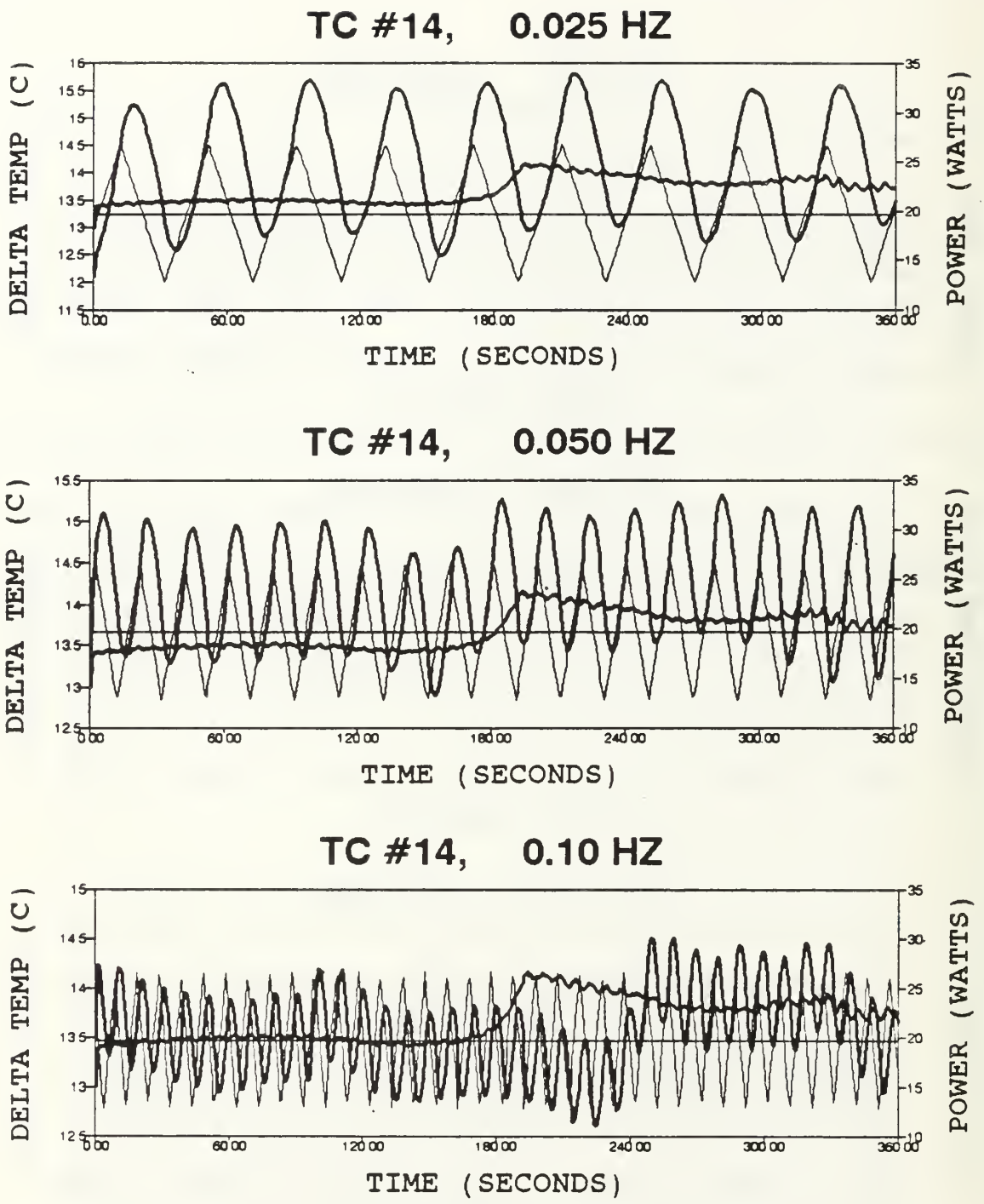

Figure 20. Delta temperature response for steady and cyclic input power with a triangular wave pattern at #14.

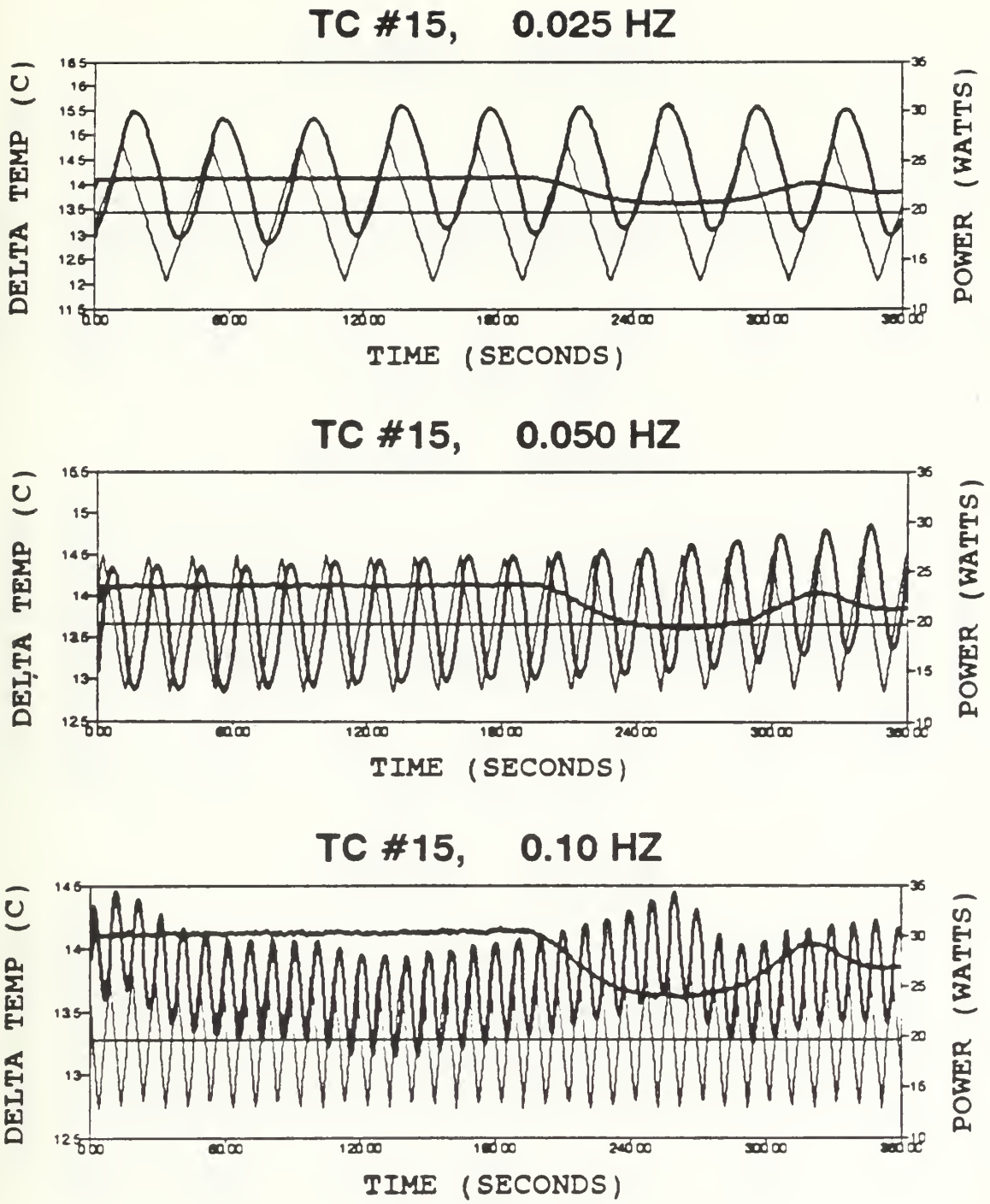

Figure 21. Delta temperature response for steady and cyclic input power with a triangular wave pattern at #15.

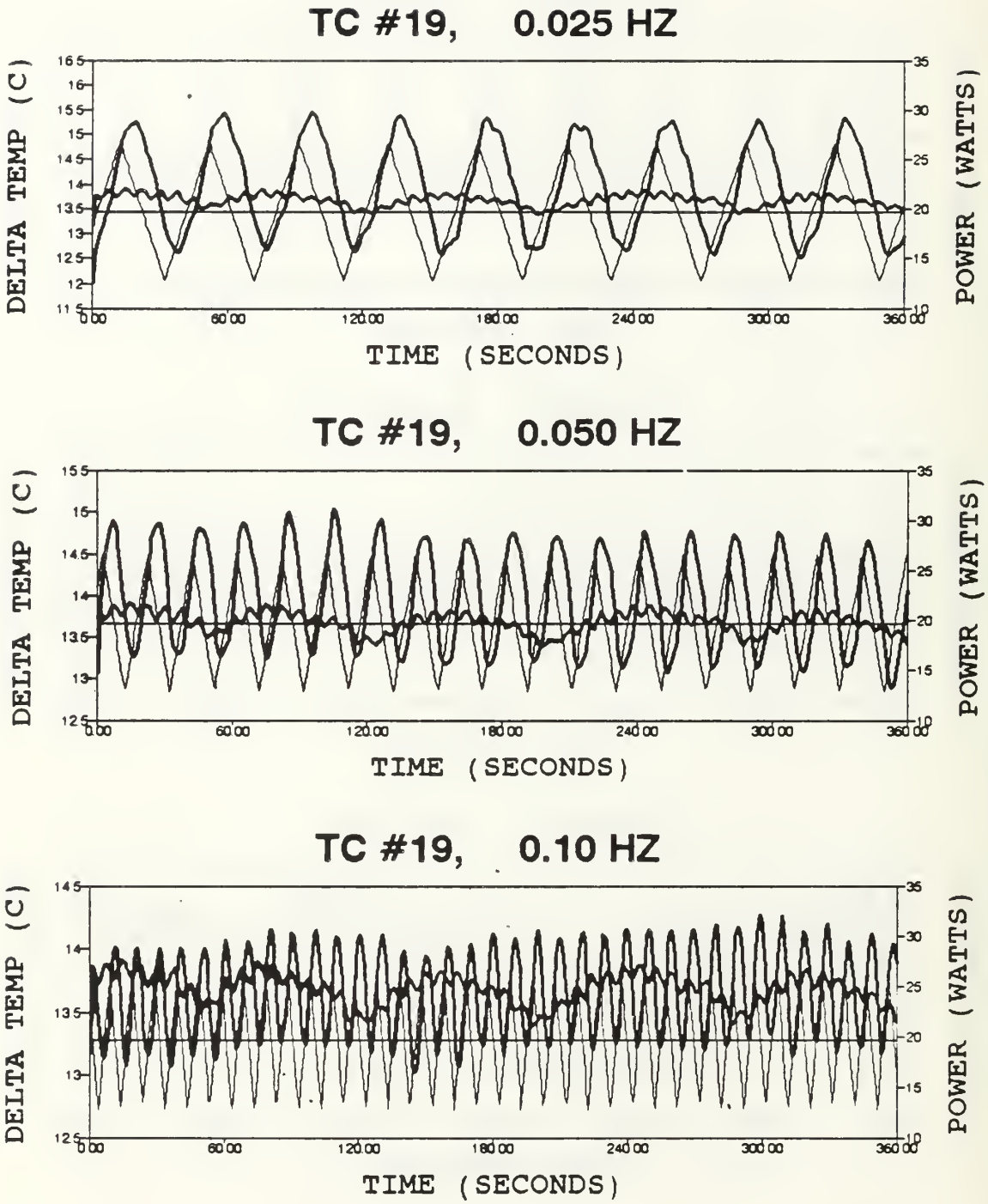

Figure 22. Delta temperature response for steady and cyclic input power with a triangular wave pattern at #19.

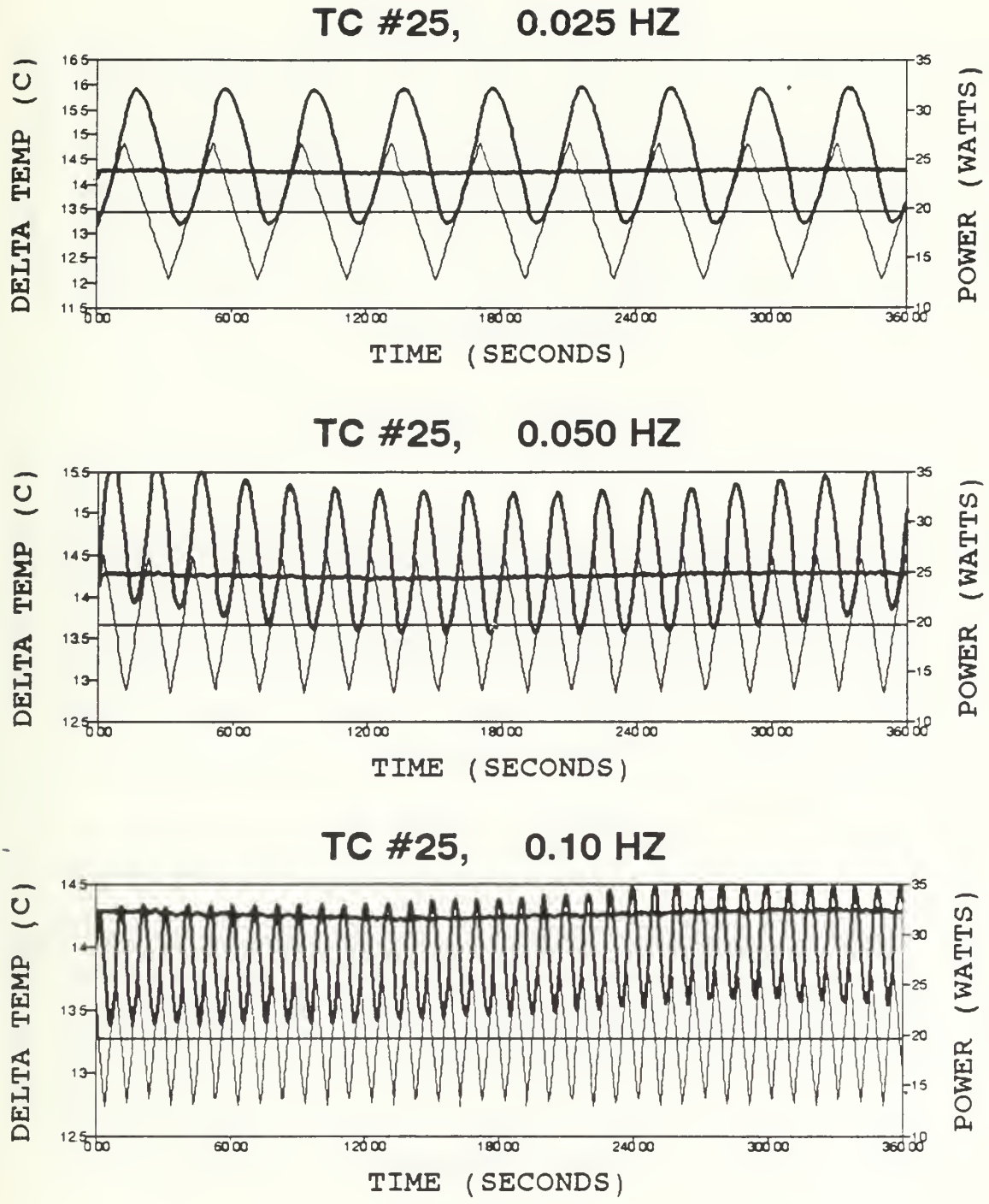

Figure 23. Delta temperature response for steady and cyclic input power with a triangular wave pattern at #25.

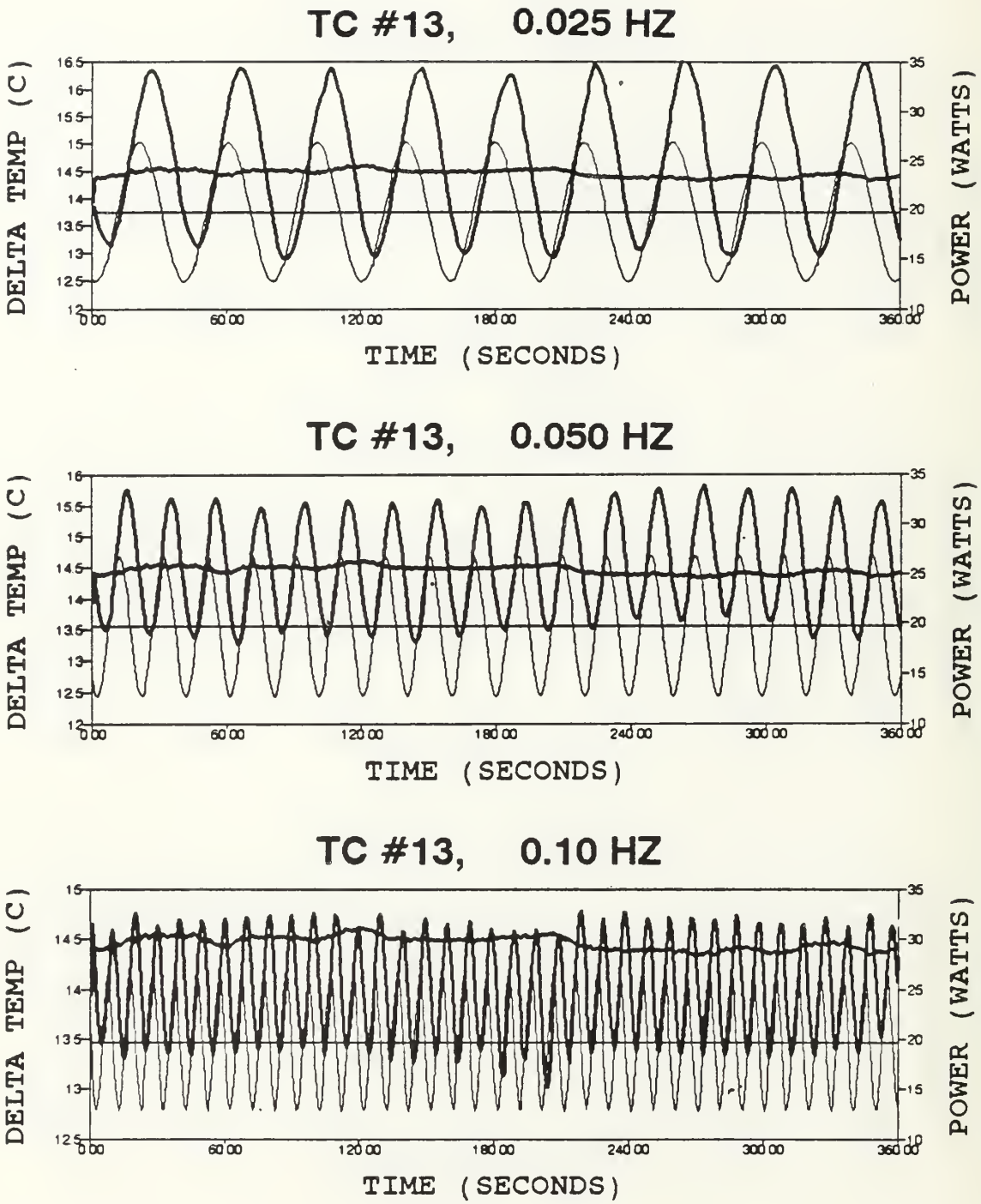

Figure 24. Delta temperature response for steady and cyclic input power with a sinusoidal wave pattern at #13.

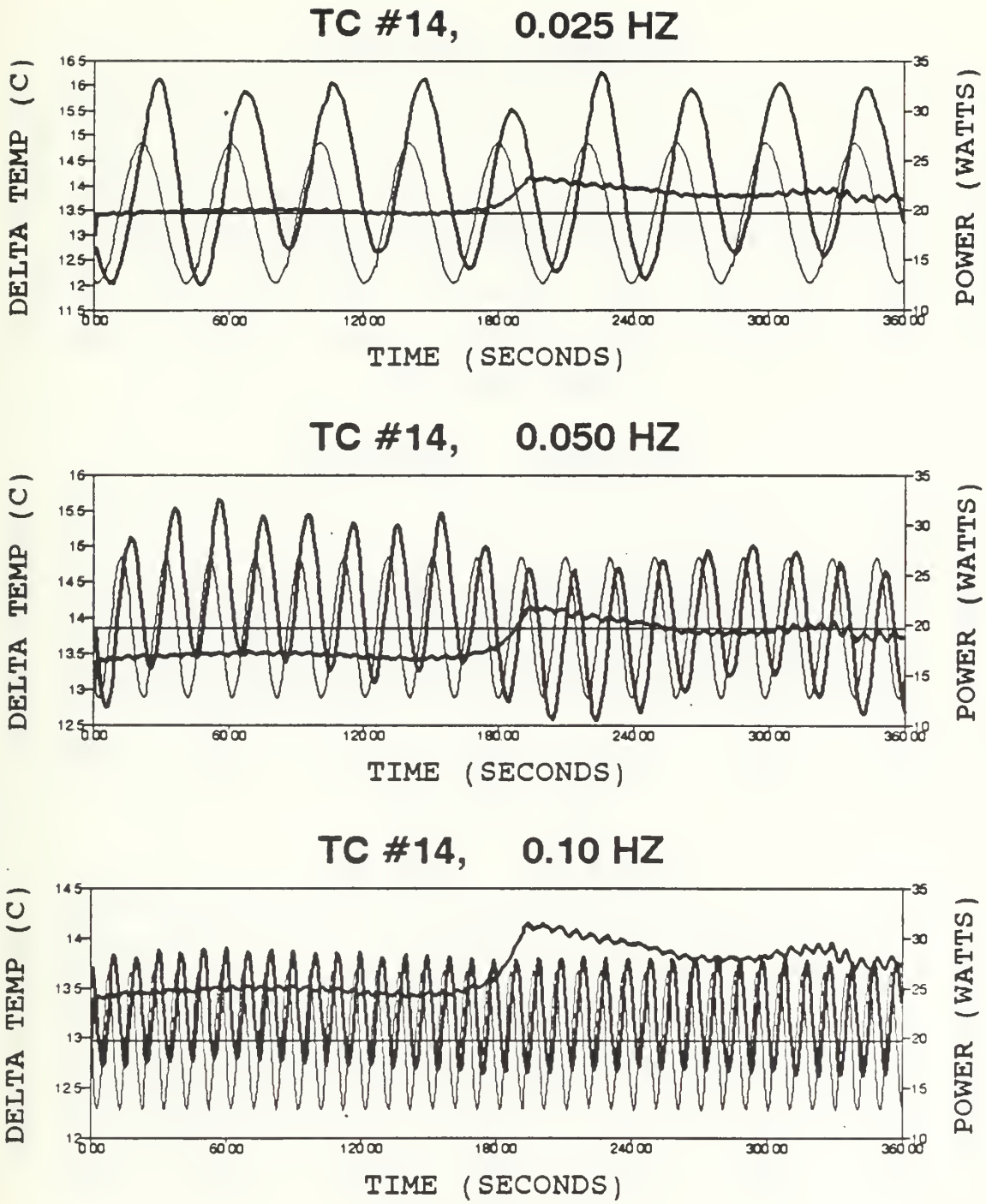

Figure 25. Delta temperature response for steady and cyclic input power with a sinusoidal wave pattern at #14.

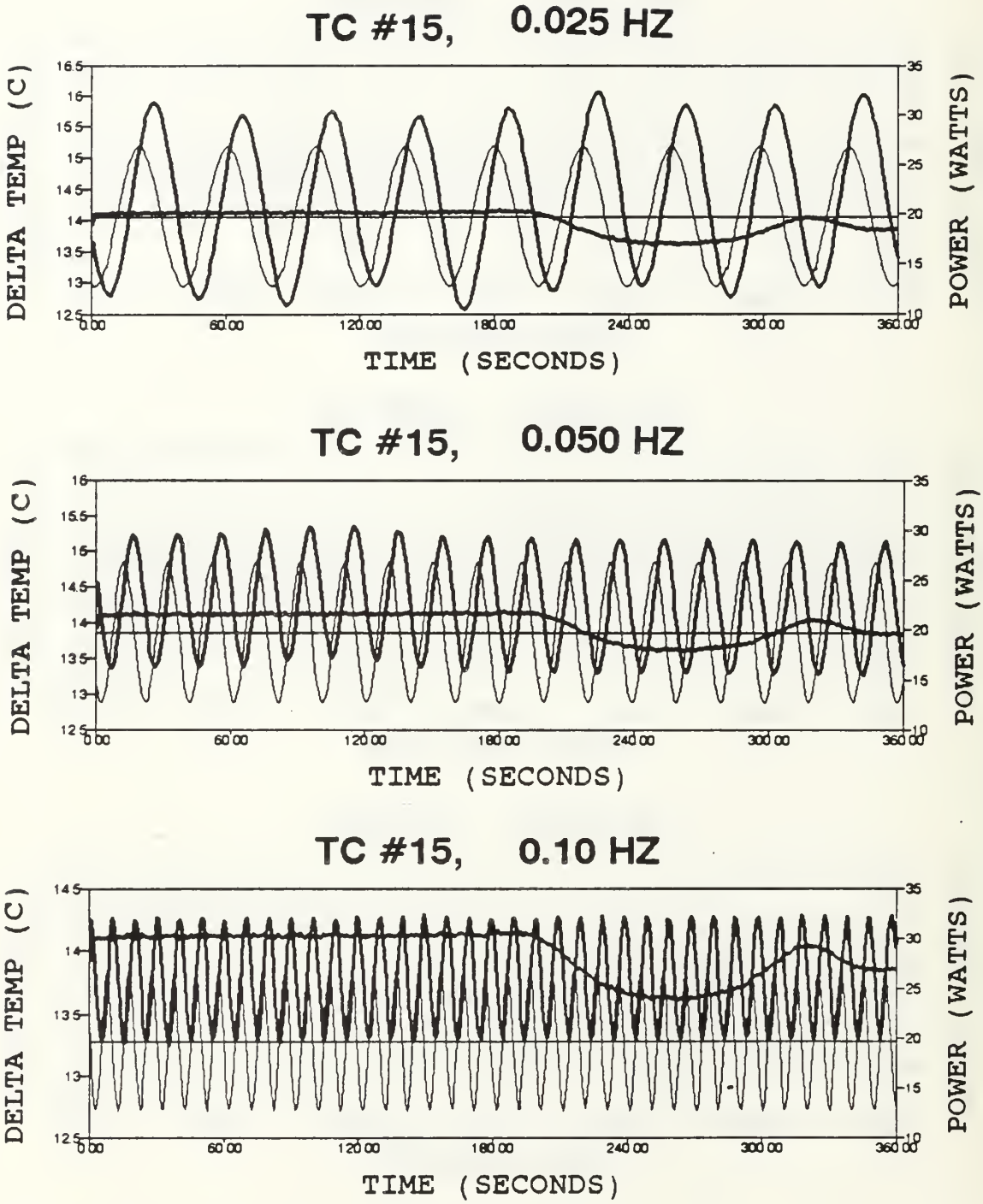

Figure 26. Delta temperature response for steady and cyclic input power with a sinusoidal wave pattern at #15.

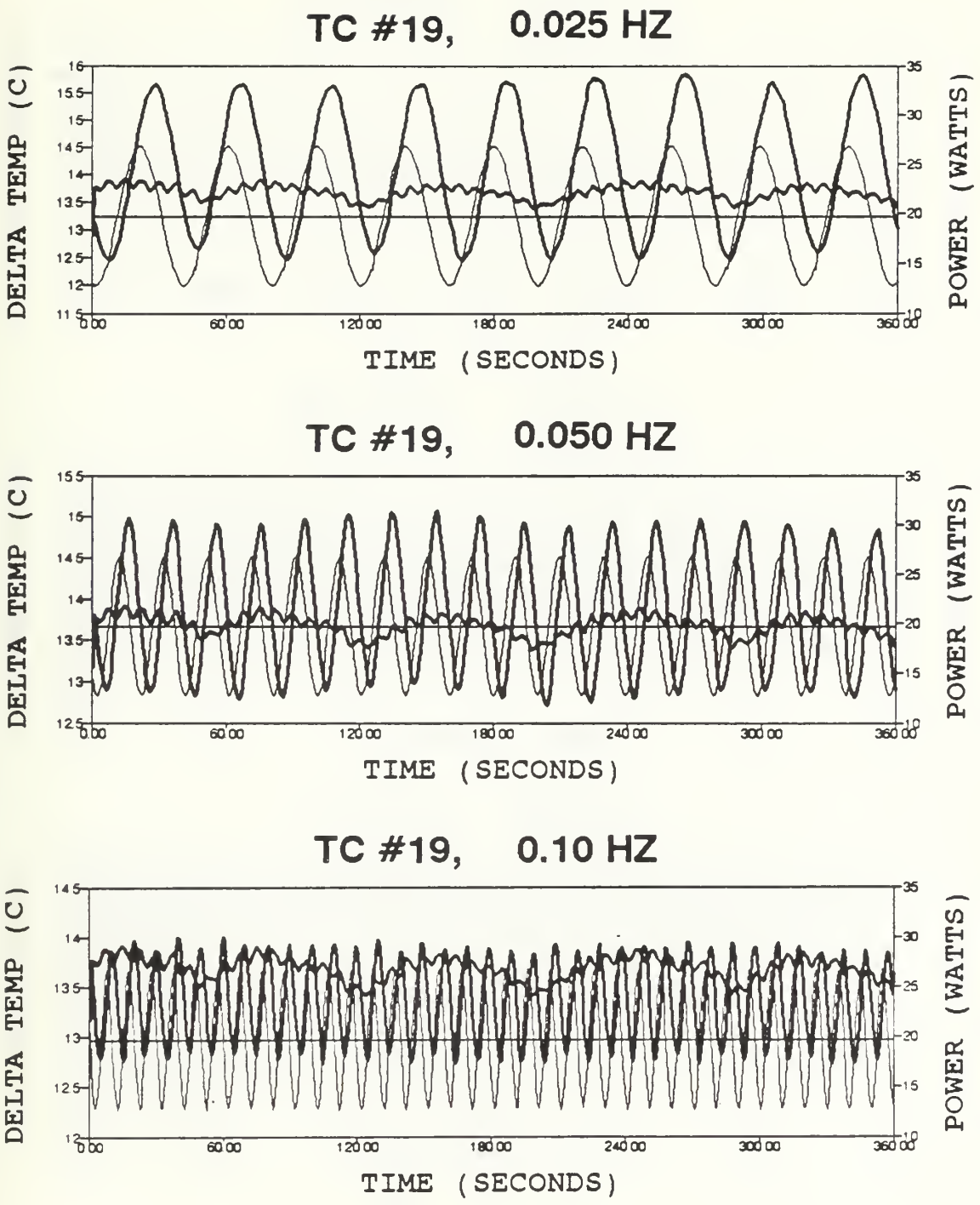

Figure 27. Delta temperature response for steady and cyclic input power a with sinusoidal wave pattern at #19.

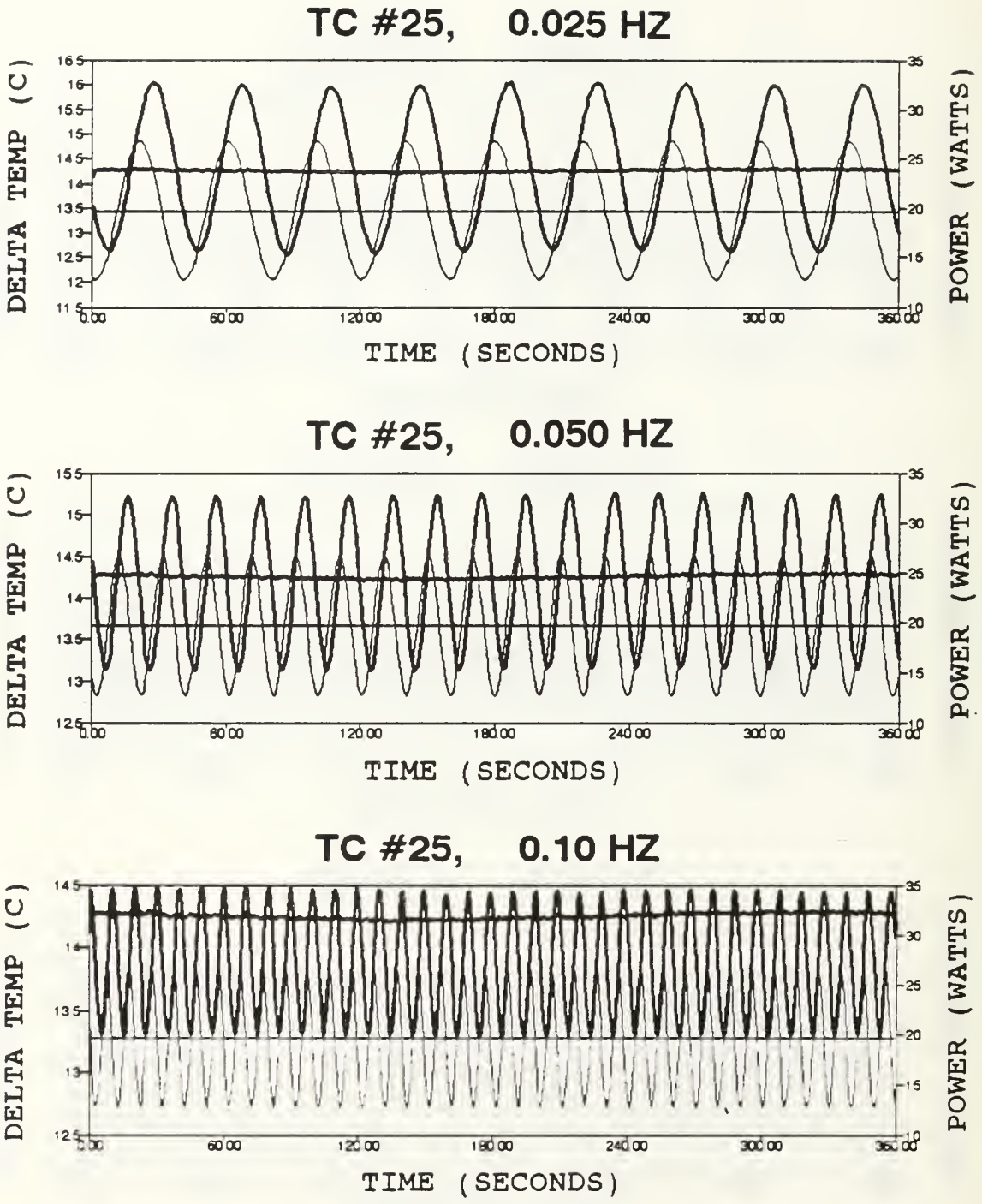

Figure 28. Delta temperature response for steady and cyclic input power with a sinusoidal wave pattern at #25.

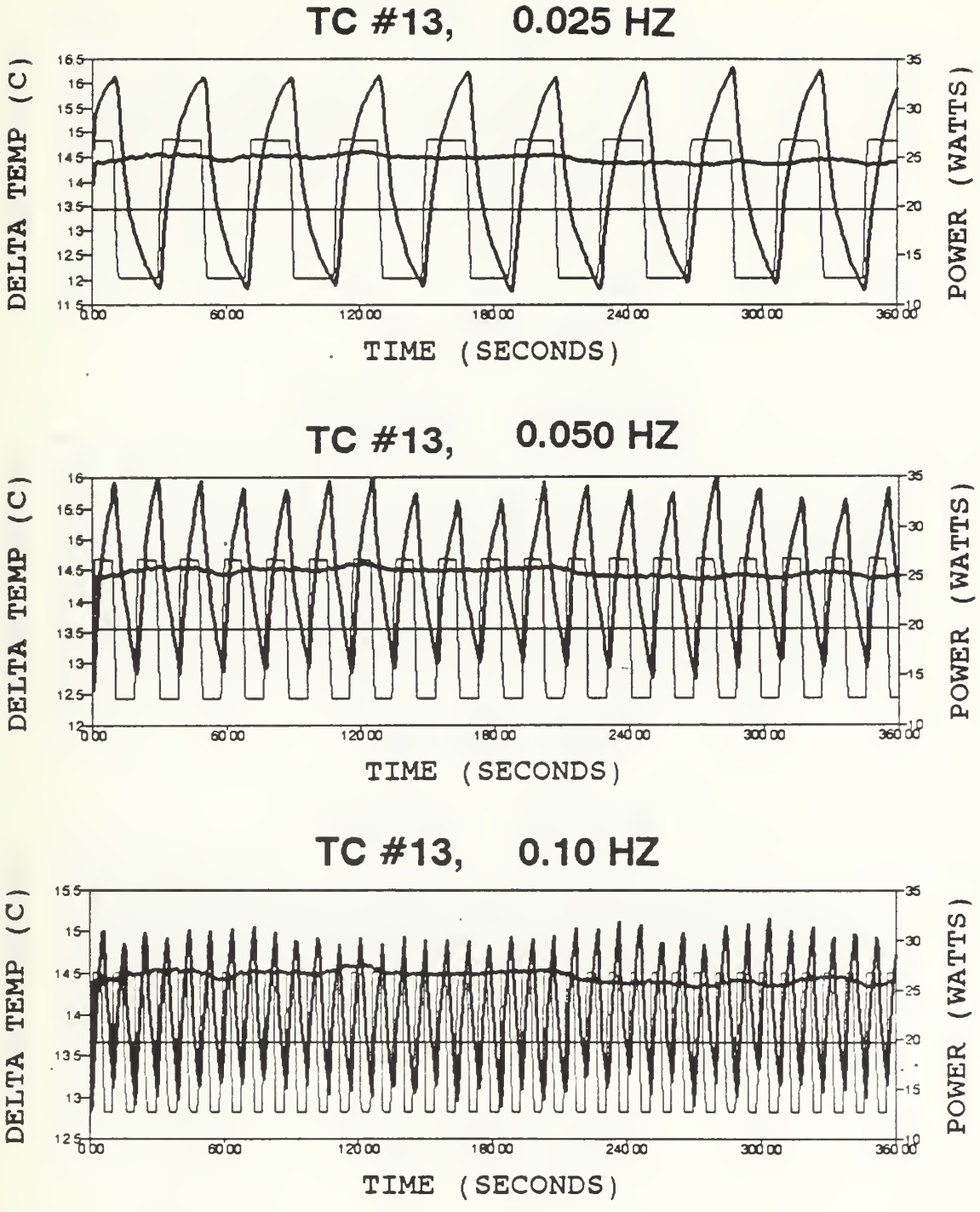

Figure 29. Delta temperature response for steady and cyclic input power with a square wave pattern at #13.

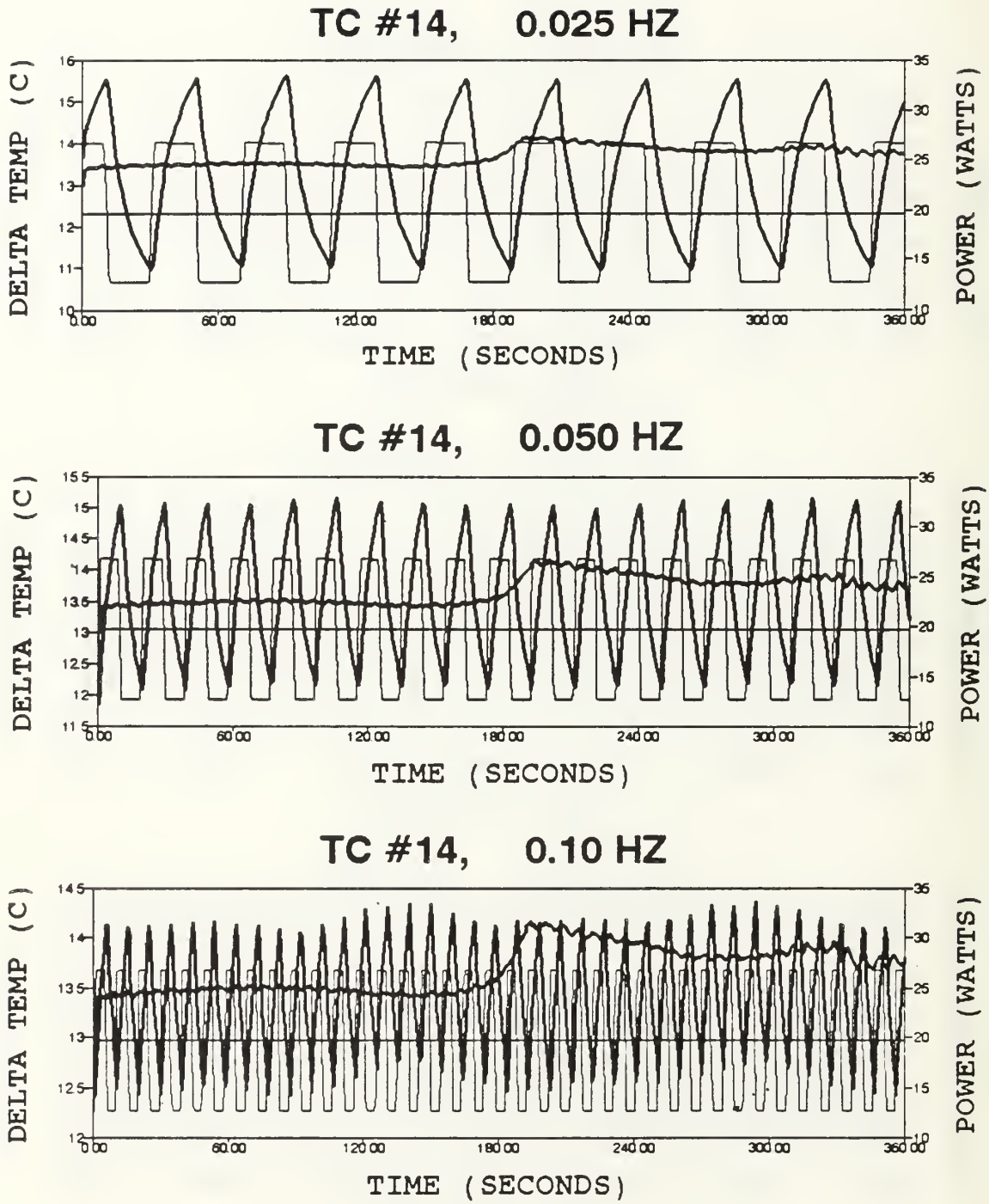

Figure 30. Delta temperature response for steady and cyclic input power with a square wave pattern at #14.

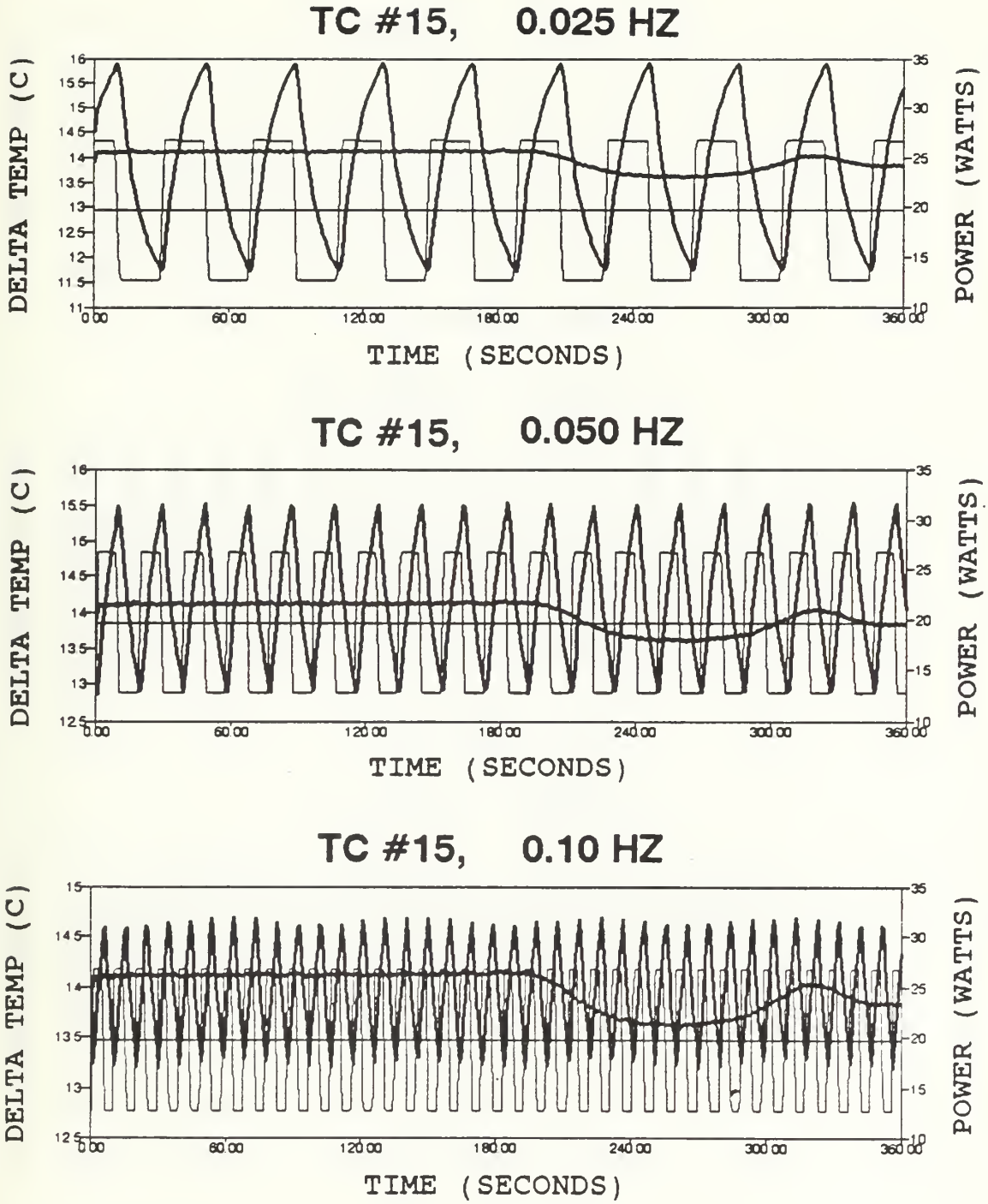

Figure 31. Delta temperature response for steady and cyclic input power with a square wave pattern at #15.

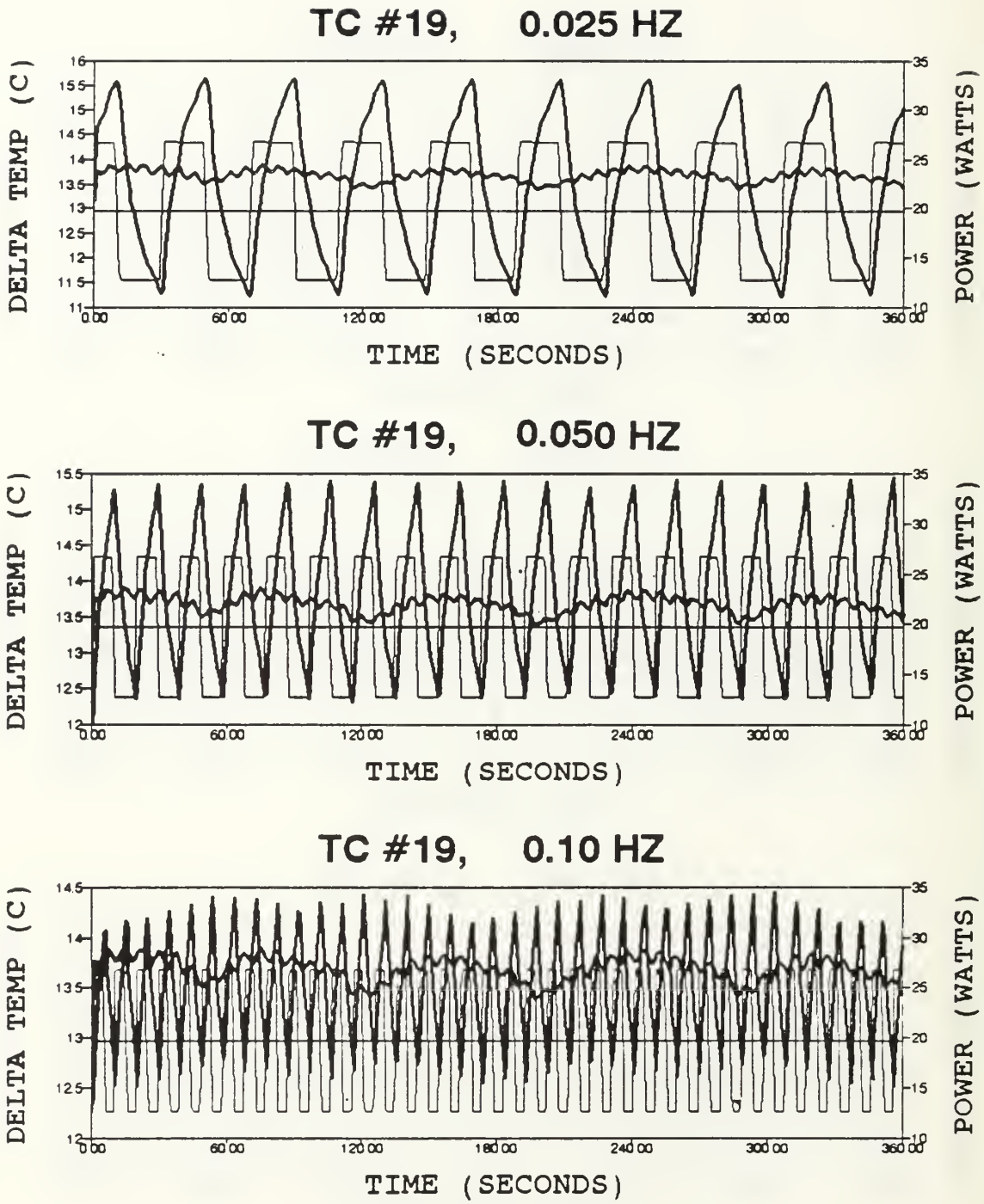

Figure 32. Delta temperature response for steady and cyclic input power with a square wave pattern at #19.

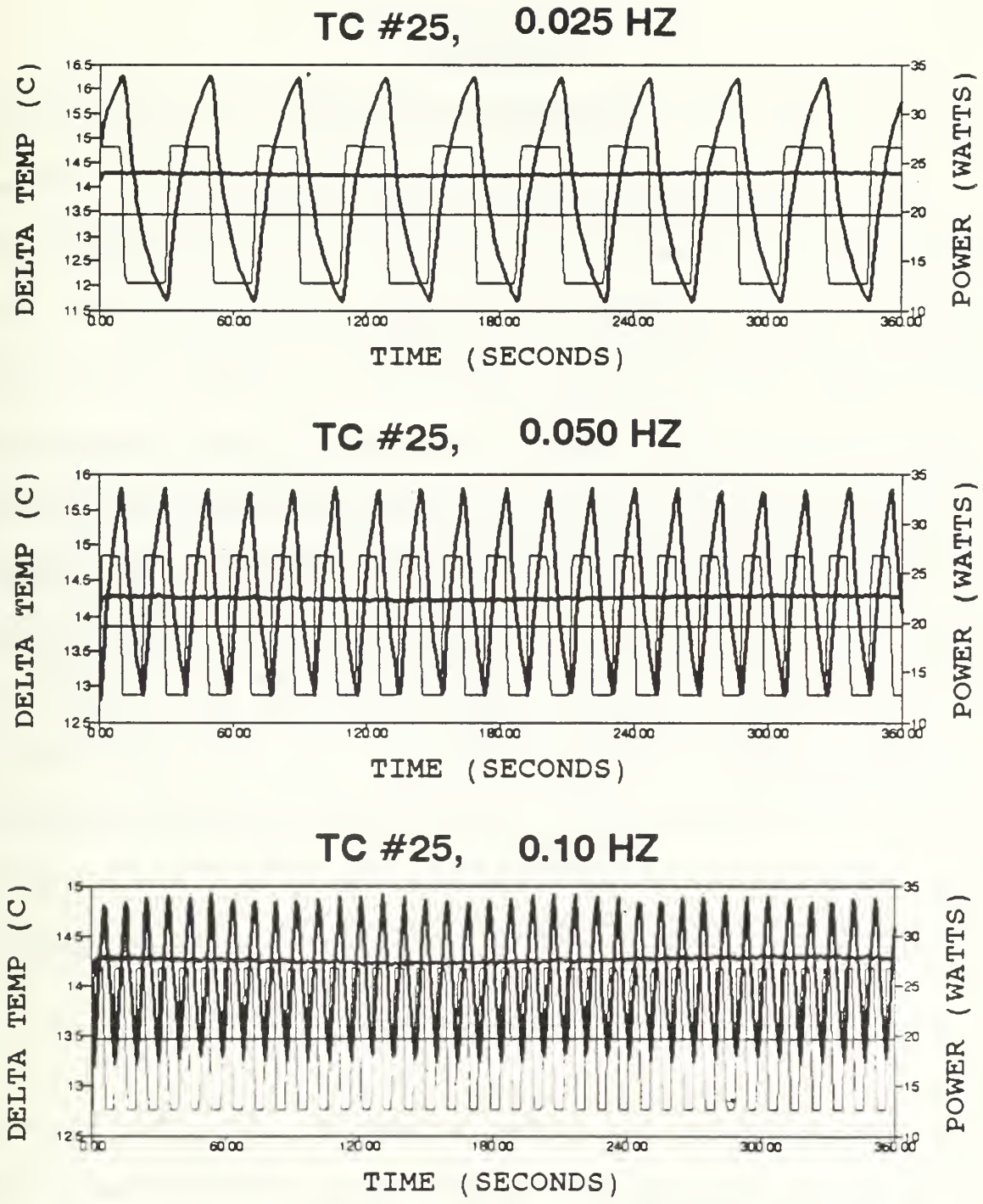

Figure 33. Delta temperature response for steady and cyclic input power with a square wave pattern at #25.

APPENDIX C

UNCERTAINTY ANALYSIS

The uncertainty in the calculated values in this investigation was determined. One half of the least count was taken to be the uncertainty in each measured quantity. The uncertainty in the power input was ± 0.001 W, in the temperature ± 0.05°C, and in the length used to determine heater dimensions ± 0.5 mm. The uncertainty analysis was done according to the approach purposed by Kline and McClintock [Ref. 19]. The uncertainty in the result R is a function of the variables in the equation and their respective uncertainties:

$$R=R(V_1, V_2, \ldots, V_n)$$

This is determined by using the expression:

$$\delta R=[((\frac{\partial R}{\partial V_1})\delta V_1)^2+((\frac{\partial R}{\partial V_2})\delta V_2)^2+((\frac{\partial R}{\partial V_n})\delta V_n)^2]^{\frac{1}{2}}$$

The uncertainties in these parameters for the present experiments were defined as δ Pwr, δ L, and $\delta\Delta$ T. Recalling that the equation for Nusselt number is:

$$N = \frac{Q_{conv} L_c}{kA(T_{plate} - T_{amb})}$$

The uncertainty of the Nusselt number was computed as follows:

$$\delta Nu = \frac{1}{K}\left[\left(\frac{L_c}{A(\Delta T)}\delta Pwr\right)^2 + \left(\frac{Pwr}{A(\Delta T)}\delta L_c\right)^2 + \left(\frac{Pwr L_c}{A^2(\Delta T)}\delta A\right)^2 + \left(\frac{Pwr L_c}{A(\Delta T)^2}\delta \Delta T\right)^2\right]^{\frac{1}{2}}$$

The above equations produced a maximum uncertainty for Nu of ± 0.22 for a nominal value of Nu=5.41. This corresponds to approximately 4.0% uncertainty. .

The above procedure was used to determine the uncertainties in RA. Without listing the equations, the maximum uncertainty for RA was ± 5.65 x 10^4 for a nominal value 1.253 x 10^6. This corresponds to approximately 4.5% uncertainty.

APPENDIX D

SAMPLE CALCULATIONS

The following calculations are based on the average temperature of 25 thermocouple locations, measured over the surface of the heater, for a time span of nine minutes, with a heat flux of 2440 W/m². The average ΔT was 13.57 °C.

1. CHARACTERISTIC DIMENSIONS

Perimeter (P) = 4(0.09)

= 0.36 m

Heater surface area (A_s) = $(0.09)^2$

= .0081 m^2

Characteristic length (L_c)=(0.0081)/(0.36)

=0.0225 m

2. CONVECTIVE HEAT FLUX

Power to heater (Q_{conv}) = 19.73 W

Heat flux (q'') = 19.73/0.0081

= 2440 W/m^2

3. WATER PROPERTIES [REF. 20]

Film temperature (T_{film}) = (32.66 + 19.09)/2 + 273.15

= 299.0 K

β = 267E-6 1/K

ν = 0.878E-6 m^2/sec

k = 0.607 W/m K

Pr = 5.985

4. NUSSELT NUMBER

Nu = (19.73)(0.0225)/(0.607)(0.0081)(13.57)

= 6.651

5. FLUX BASED RAYLEIGH NUMBER

$$Ra = \frac{(9.81)(267E\text{-}6)(19.73)(0.0225)^4}{(0.607)(0.0081)(0.878E\text{-}6)^2} 5.985$$

= 20.911E+6

6. TEMPERATURE BASED RAYLEIGH NUMBER

$$Ra = \frac{(9.81)(267E\text{-}6)(13.57)(0.0225)^3}{(0.878E\text{-}6)^2} 5.985$$

= 3.143E+6

LIST OF REFERENCES

1. Chu, R.C., "Heat Transfer in Electronic Systems," *The Eighth Int Heat Transfer Conf. Proceedings*, v.I, 1986.

2. Bar-Cohen, A., and Kraus, A.D., *Advances in Thermal Modeling of Electronic Components and Systems*, ASME Press, 1990.

3. Bar-Cohen, A., "Thermal Management of Electronic Components with Dielectric Liquids," *ASME/JSME Thermal Engineering Proceedings*, v.2, pp. xv-xxxi, ASME 1991.

4. Sathe, S.B., and Joshi, Y., "Natural Convection Arising From A Heat Generating Substrate-Mounted Protrusion in a Liquid-Filled Two-Dimensional Enclosure," *Int J. Heat Mass Transfer*, v.34, No.8, pp. 2149-2163, 1991.

5. Incropera, F.P., "Convection Heat Transfer in Electronic Equipment Cooling," *AMSE Journal of Heat Transfer*, v.110, pp. 1097-1111, 1988.

6. Joshi, Y., Kelleher, M., and Benedict, T., "Natural Convection Immersion Cooling of an Array of Simulated Chips in an Enclosure Filled With Dielectric Fluid," Presented at the XXth International Symposium of the International Center for Heat and Mass Transfer, Dubrovnic, Yugoslavia, 1988.

7. Kelleher, M., Knock, R., and Yang, K., "Laminar Natural Convection in a Rectangular Enclosure Due to a Heated Protrusion on a Vertical Wall Part I: Experimental Investigation,"*Proc. Second ASME/JSME Therm. Engr. Joint Conf.*, Honolulu, pp.167-177, 1987.

8. Lee, K., Kelleher, M., Knock, R., and Yang, K., "Laminar Natural Convection in a Rectangular Enclosure Due to a Heated Protrusion on a Vertical Wall Part II: Numerical

Simulations," *Proc. Second ASME/JSME Therm. Engr. Joint Conf.*, Honolulu, pp.167-177, 1987.

9. Oosthuizen, P.H., Paul, J.T., "Natural Convection Heat Transfer From a Square Element Mounted on the Wall of an Inclined Square Enclosure'" AIAA 22nd Thermophysics Conference, Honolulu, 1987.

10. Joshi,Y., and Knight, L., "Natural Convection From a Column of Flush Heat Sources in a Vertical Channel in Water," *Journal of Electronic Packaging*, v. 112,pp. 367-374, December 1990.

11. Gaiser, Alfred O.,"Natural Convection Liquid Immersion Cooling of High Density Columns of Discrete Heat Sources in a Vertical Channel," Master's Thesis, Naval Postgraduate School, Monterey, California, June 1989.

12. Haukenes, Larry O.,"A Computational and Experimental Study of Flush Heat Sources in Liquids," Master's Thesis, Naval Postgraduate School, Monterey, California, June 1990.

13. Akdeniz, Erhan M., "Effects of Power Pulsations On Natural Convection From Discrete Heat Sources," Master's Thesis, Naval Postgraduate School, Monterey, California, March 1991.

14. Larsen, Steven, "Effects of Power Pulsations On Natural Convection From Discrete Heat Sources," Master's Thesis, Naval Postgraduate School, Monterey, California, December 1991.

15. Goldstein, R.L., Sparrow, E.M., Jones D.C., "Natural Convection Mass Transfer Adjacent to Horizontal Plates," *Int. J. Heat Mass Transfer*,v.16,pp. 1025-1035, 1973.

16. Lloyd, J.R., and Moran, W.R., "Natural convection Adjacent to Horizontal Surface of Various Planforms,"*J. Heat Transfer*, v.96, pp. 443-447, 1974.

17. Husar, R.B., and Sparrow, E.M., "Patterns of Free Convection Flow Adjacent To Horizontal Heated Surfaces," *Int. J. Heat Mass Transfer*, v.11, pp. 1206-1208, 1968.

18. Ackroyd, J.A.D., "Laminar Natural Convection Boundary Layers on Near-Horizontal Plates," *Proc. R. Soc. London Ser. A*, v.352, pp. 249-274, 1976.

19. Kline, S.J., and McClintock, F.A., "Describing Uncertainties in Single Sample Experiments," *Mechanical Engineering*, January, 1953.

20. Incropera, F.P., and Dewitt, D.P., *Introduction to Heat Transfer*, John Wiley & Sons, Inc., 1985.

INITIAL DISTRIBUTION LIST

		Copies
1.	Defense Technical Information Center Cameron Station Alexandria, Virginia 22304-6145	2
2.	Library, Code 0142 Naval Postgraduate School Monterey, California 93943-5002	2
3.	Prof. A.J. Healey, Code ME/Hy Department of Mechanical Engineering Naval Postgraduate School Monterey, California 93943-5002	1
4.	Prof. Y. Joshi, Code ME/Ji Department of Mechanical Engineering Naval Postgraduate School Monterey, California 93943-5002	2
5.	Mr. Kip Hoffer Naval Weapons Support Center Code 6042 Crane, Indiana 47522	1
6.	Mr. Tony Buechler Naval Weapons Support Center Code 6042 Crane, Indiana 47522	1
7.	Naval Engineering Curricular Office, Code 34 Naval Postgraduate School Monterey, California 93943-5002	1
8.	Christopher N. Hickey C/O Norman W. Hickey Bay Front Towers 1 Beach Drive SE Apt 2711 St. Petersburg, Florida 33701	1